Strain signals governed by frictional-elastoplastic interaction of the upper plate and shallow subduction megathrust interface over seismic cycles

Ehsan Kosari [1,2†], Matthias Rosenau [1], Onno Oncken [1,2]

[1]Helmholtz Centre Potsdam, GFZ German Research Centre for Geosciences, Potsdam, Germany.

[2]Department of Earth Sciences, Freie Universität Berlin, Berlin, Germany.

†Corresponding author: Ehsan Kosari (ehsan.kosari@gfz-potsdam.de)

Key Points:

- Analog earthquake cycle experiments provide observations to evaluate the surface strain signals from the shallow megathrust.
- The extensional segment of the forearc overlays the seismogenic zone at depth.
- The strain state may remain quasi-stable over a few seismic cycles in the coastal zone.

Abstract

Understanding the behavior of the shallow portion of the subduction zone, which generates the largest earthquakes and devastating tsunamis, is a vital step forward in the earthquake geoscience. Monitoring only a fraction of a single megathrust earthquake cycle and the offshore location of the source of these earthquakes are the foremost reasons for the insufficient understanding. The frictional-elastoplastic interaction between the interface and its overlying wedge causes variable surface strain signals such that the wedge strain patterns may reveal the mechanical state of the interface. We employ Seismotectonic Scale Modeling and simplify elastoplastic megathrust subduction, generate hundreds of analog seismic cycles at laboratory scale, and monitor the surface strain signals over the model's forearc over high to low temporal resolutions. We establish two coseismically compressional and extensional wedge configurations to explore the mechanical and kinematic interaction between the shallow wedge and the interface. Our results demonstrate that this interaction can partition the wedge into different segments such that the anlastic extensional segment overlays the seismogenic zone at depth. Moreover, the different segments of the wedge may switch their state from compression/extension to extension/compression domains. We highlight that a more segmented upper plate represents megathrust subduction that generates more characteristic and periodic events. Additionally, the strain time series reveals that the strain state may remain quasi-stable over a few seismic cycles in the coastal zone and then switch to the opposite mode. These observations are crucial for evaluating earthquake-related morphotectonic markers (i.e., marine terraces) and short-term interseismic GPS time-series onshore (coastal region).

1 Introduction

Estimating the interseismic coupling is the foremost approach to evaluate the earthquake potential of subduction megathrusts (e.g., Chlieh et al., 2008; Moreno et al., 2010; Wallace et al., 2012; McCaffrey et al., 2013; Métois et al., 2013; Schmalzle et al., 2014). While both up-dip and down-dip limits of megathrust ruptures are typically located offshore and near the shore, respectively, centuries-long recurrence intervals of the subduction megathrust earthquakes and geodetically insufficiently instrumented seafloors prevent us from achieving sufficient details of the shallow part of the megathrust (Kosari et al., 2020; Williamson & Newman, 2018). For instance, a weakly coupled interface had been predicted in NE Japan based on the incomplete interseismic geodetic measurements before the 2011 Tohoku-Oki megathrust event (e.g., Loveless & Meade, 2011).

However, the slip models of the earthquake itself derived from rare offshore geodetic data suggested a coseismic trench-breaching rupture (e.g., Ozawa et al., 2011; Simons et al., 2011; Sun, Wang, Fujiwara, Kodaira, & He, 2017). Besides short-term (geodetic) elastic surface deformation information, it is considered worthwhile to explore long-term (geologic) permanent deformation signals for potential diagnostic patterns linked to megathrust behavior (Geersen et al., 2018; Jara-Muñoz et al., 2015; Madella & Ehlers, 2021; Malatesta et al., 2021; Melnick et al., 2018; Molina et al., 2021; Normand et al., 2019; Ott et al., 2019; Saillard et al., 2017). Hence, for the sake of completeness of seismotectonic insights, long-term geological information should be referred to.

Elastoplastic deformation is the dominant process in the shallow portion of the subduction zones (Wang & Hu, 2006), and the mechanical properties of the wedge and megathrust govern the strain pattern in the upper plate. The strain signals could be accumulated over a single or many seismic cycles and preserved as morphotectonic features (i.e., extensional, compressional, and shear markers) (Baker et al., 2013; Delano et al., 2017; Loveless et al., 2009; Loveless et al., 2010; Rosenau & Oncken, 2009), representing the mechanical state of the forearc (Cubas et al., 2013a and 2013b). In an earthquake cycle, the mechanical state might be highly variable in the upper plate (Kopp, 2013; Melnick et al., 2009). In other words, the rate-strengthening and rate-weakening portions of the megathrust cause time and space variable strain fields and rates over the forearc during a seismic cycle. For instance, the coastal region can typically be under compression during the interseismic period and under extension during and immediately following the coseismic stage. Understanding how this leads to coastal topography and offshore bathymetry as a persistent marker over many seismic cycles is vital. Eventually, this may lead to incremental upper plate evolution towards its critical geometry and shape the forearc morphology (Cubas et al., 2013a and 2016; Wang & Hu, 2006).

It is not fully transparent that to what extent we may infer the seismic potential of the shallow (offshore) portion of the megathrust via onshore observations. Furthermore, the potential temporal linkage between strain states (elastic and plastic) at the positions of the coast, inner-, and outer-wedge is not resolved. Finally, could permanent surface deformation (i.e., plastic strain) be reliably used as a clue for inferring the zones with megathrust earthquake potential? In an attempt to answer these questions, we employ Seismotectonic Scale Modeling (Rosenau et al., 2017 and 2009) to generate physically self-consistent analog megathrust earthquake ruptures and seismic cycles at the laboratory scale (Figure 1).

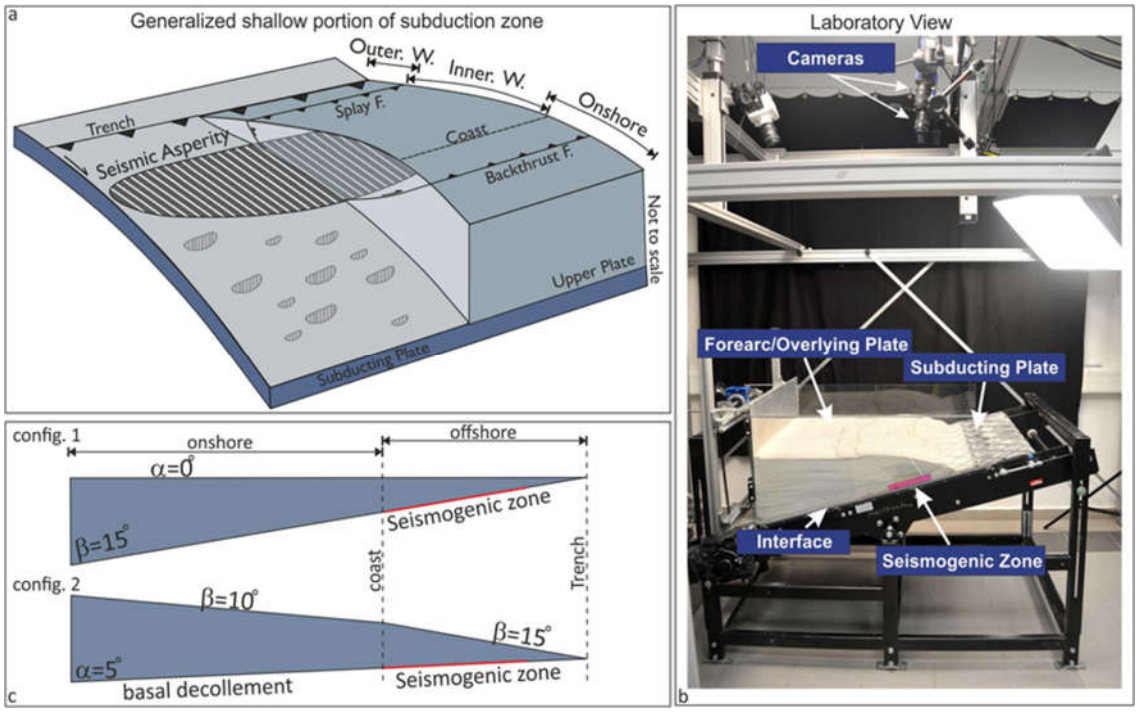

Figure 1: a: Generalized shallow portion of the subduction zone. The structures in the upper plate and subducting plate are simplified. This schematic has been considered as a base for our analog seismotectonic model. b: Laboratory view of our experiment. The main part of the analog model is labeled in the image. c: 2d view of the two evaluated configurations in this study. The projection of the down-dip limit of the stick-slip materials is defined as the coastal area. Alpha (α) and beta (β) represent the surface and basal decollement, respectively.

This method has been used to study the interplay between short-term elastic (seismic) and long-term permanent deformation (Rosenau and Oncken 2009). For mimicking the megathrust seismic cycle and its associated surface deformation, we use a zone of velocity weakening (stick-slip) and an elastoplastic wedge while the wedge is continuously compressed via a basal conveyor belt (Kosari et al., 2020; Rosenau et al., 2019). A stereoscopic image correlation technique has been used to monitor the surface deformation of the analog model (Adam et al., 2005). Generating hundreds of seismic cycles and monitoring the associated surface deformation allows us to unwrap the surface signals related to frictional properties at depth (velocity weakening versus velocity strengthening).

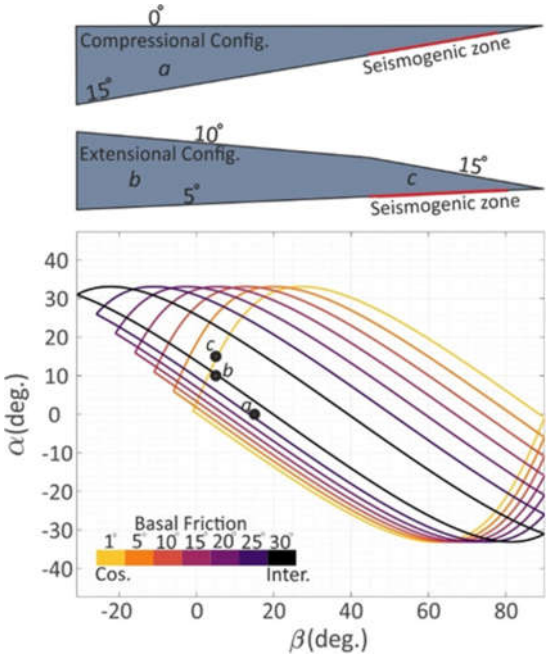

Figure 2: Mechanical states of a wedge introduced by the critical taper theory for coseismically compressional and extensional experiments. The areas within the envelopes characterize stable regimes. The areas above and below the envelopes indicate unstable extensional and compressional regimes, respectively. The positions on the envelopes represent critically stable domains.

2 Seismotectonic Scale Modeling and Monitoring Techniques

Seismotectonic scale modeling is a unique technique to forward model the tectonic evolution over seismic cycles (e.g., Rosenau et al., 2017, and references therein). The approach has been used to study the interplay between short-term elastic (seismic) and long-term permanent deformation (Rosenau & Oncken, 2009), earthquake recurrence behavior and predictability (Corbi et al., 2020; 2019; 2017; Rosenau et al., 2019), the linkage between offshore geodetic coverage and coseismic slip models (Kosari et al., 2020) and details of the seismic cycle (Caniven & Dominguez, 2021). Analog models are downscaled from nature for the dimensions of mass, length, and time to maintain geometric, kinematic, and dynamic similarity by applying a set of dimensionless numbers (King Hubbert, 1937; Rosenau et al., 2009; 2017). The models generate a sequence of tens to hundreds of analog megathrust earthquake cycles, allowing the analysis of the corresponding surface displacement from dynamic coseismic to quasi-static interseismic stages.

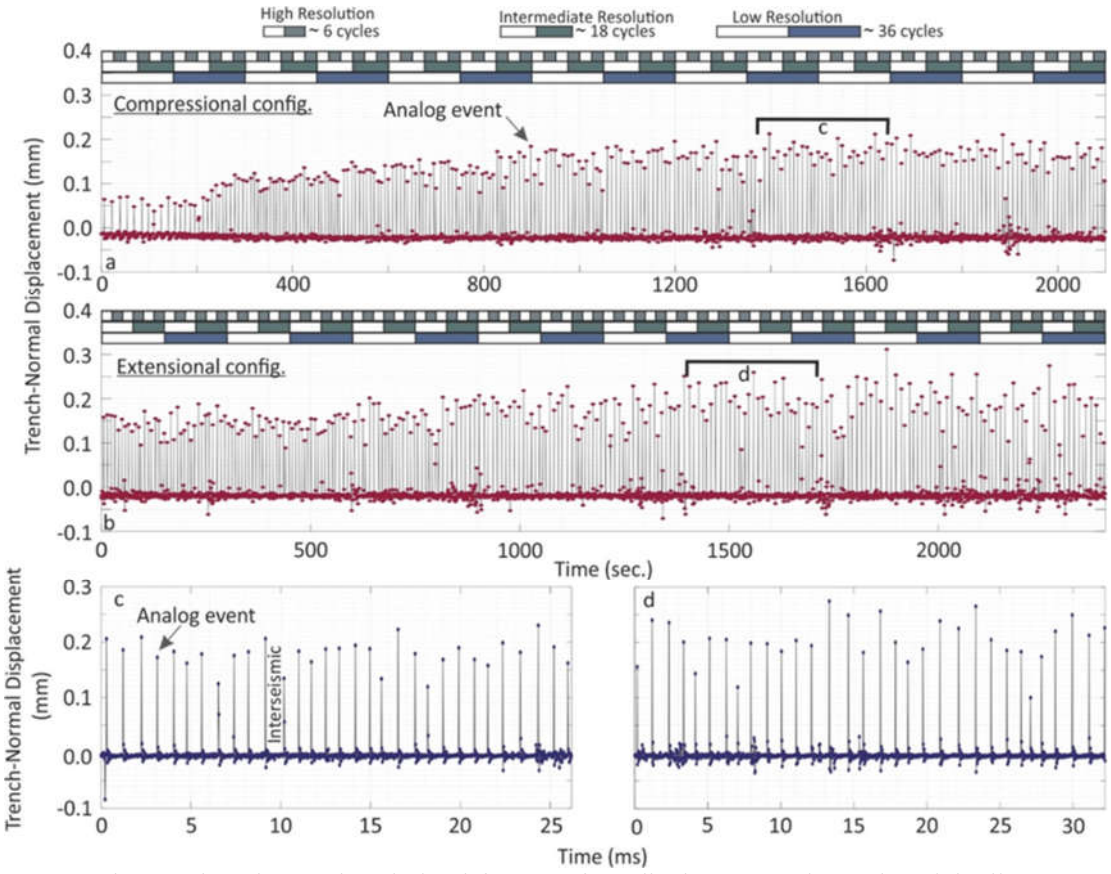

Figure 3: Analog earthquake catalog derived from surface displacement above the stick-slip zone on the model surface. The displacements larger than 0.05 millimeters represent an analog megathrust event (Mw≥8 at nature scale). Distance between two analog events represents the interseismic period in our experiments. a and b: all the events that occurred over model evolution from compressional and extensional experiments, respectively. Temporal processing windows for three different resolutions are differentiated by scale bars (see figures 7 and 8 for more details).c and d: a selected set of 30-32 analog megathrust events for evaluating surface displacement over the seismic cycles from both configurations, respectively.

In the 3-D experimental setup introduced in Kosari et al. (2020), a subduction forearc model is set up in a glass-sided box (1,000 mm across strike, 800 mm along strike, and 300 mm deep) on top of an elastic basal rubber conveyor belt (the model slab), and a rigid backwall. A wedge made of an elastoplastic sand-rubber mixture (50 vol.% quartz sand G12: 50 vol.% EPDM-rubber) is sieved into the setup representing a 240 km long forearc segment from the trench to the volcanic arc position (Figure 1).

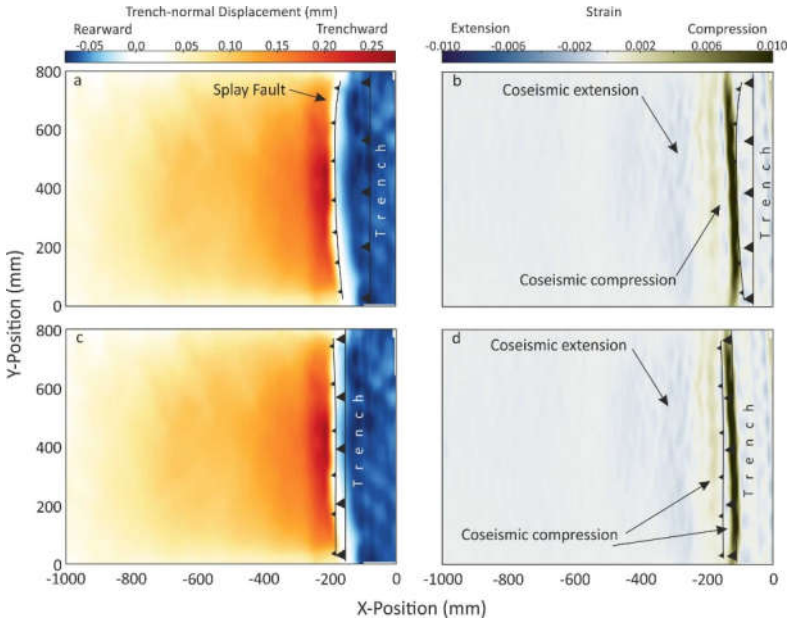

Figure 4: Surface horizontal displacement (a and c) and strain (b and d) maps derived from the extensional configuration. The upper panel represents the case of a megathrust event in which slip propagates on the splay faults (non-trench-reaching). The lower panel represents a megathrust event in which the slip reaches the trench (trench-reaching slip). The compressional (outer-wedge) and extensional (inner-wedge) segments.

At the base of the wedge, zones of velocity weakening controlling stick-slip ("seismic" behavior) are realized by emplacing compartments of "sticky" rice ("seismogenic zone"), which generate quasi-periodic slip instabilities while sheared continuously (Figure 1), mimicking megathrust earthquakes of different sizes and frequency (Figure 3). Large stick-slip instabilities are assumed to represent almost complete stress drops and recur at low frequency (~0.2 Hz) at a prescribed constant convergence rate of 50 µm/s. This stick-slip behavior is intended to mimic rare great (M8-9) earthquakes with century-long recurrence intervals. The wedge itself and the conveyer belt respond elastically to these basal slip events similar to crustal rebound during natural subduction megathrust earthquakes. Upper plate faults (in our case, an "inland" backthrust fault and "offshore" forethrust and backthrust faults) emerge self-consistently downdip and up-dip of the seismogenic zone over multiple seismic cycles, as the effect of transient compression as documented in earlier papers (Kosari et al., 2020; Rosenau et al., 2009, 2010; Rosenau & Oncken, 2009).

Two different wedge geometries have been realized: a compressional configuration represents a transiently compressional wedge, and an extensional configuration, which is transiently extensional according to Coulomb wedge theory (Figure 2). In the first configuration, hereafter

named “compressional configuration”, a flat-top (α=0) elastoplastic wedge overlies a single large rectangular in map view stick-slip patch (Width*Length=200*800 mm) over a 15-degree dipping conveyor belt. In the second configuration, hereafter named “extensional configuration”, the surface angle of the elastoplastic wedge varies from onshore (α=10) to offshore (α=15) segments over a 5-degree basal decollement. The stick-slip zone in both configurations represents a system of a homogeneous seismogenic zone with a temperature-controlled depth range and no variation along strike generating M9 type megathrust events (Figure 1). According to Coulomb wedge theory (Dahlen et al., 1984), the shallow wedge part of the compressional configuration overlying the seismogenic zone is compressional in the interseismic stage when the basal friction angle in the seismogenic zone is high (about 30°) and stable during the coseismic stage when the basal friction in the seismogenic zone drops to zero. The coastal part of the wedge in the compressional configuration is compressional throughout the seismic cycle as the basal friction is high and rate-independent here. The extensional configuration, in contrast, has a coastal wedge that is stable throughout the seismic cycle, whereas the shallow wedge overlying the seismogenic zone is stable interseismically but becomes extensional during the coseismic stage. Both models produce trench-reaching and non-trench-reaching slip analog megathrust events and push their overlying wedges to compressional and extensional strain states (Figure 4).

To capture horizontal micrometer-scale surface displacements associated with analog earthquakes and interseismic intervals at microsecond scale periods, a stereoscopic set of two CCD (charge-coupled device) cameras (LaVision Imager pro X 11MPx, 14 bit) images the wedge surface continuously at 4 Hz. To derive observational data similar to those from geodetic techniques, that is, velocities (or incremental displacements) at locations on the model surface, we use digital image correlation (DIC) (Adam et al., 2005) via the DAVIS 10 software (LaVision GmbH, Göttingen/DE) and derive the 3-D incremental surface displacements at high resolution (<0.1 mm) (Figure 3).

To calculate strain, we use the infinitesimal strain tensor because the condition of small strain is met when resolving strains across the forearc during the interseismic period:

$$\begin{pmatrix} \varepsilon_{xx} & \varepsilon_{xy} & \varepsilon_{xz} \\ \varepsilon_{yx} & \varepsilon_{yy} & \varepsilon_{yz} \\ \varepsilon_{zx} & \varepsilon_{zy} & \varepsilon_{zz} \end{pmatrix}$$

where ε_{xx} represent the partial derivation of the trench-normal surface velocity component $\frac{\partial V_x}{\partial x}$ showing trench-normal shortening: positive and negative values respectively represent compression and extension.

3 Results and Interpretations

The models' observations are presented in succession from long-term to short-term. First, we show how the upper plate structures evolve in a sequence over hundreds of analog earthquake cycles. We evaluate the spatial correlation between upper plate strain and topography evolution concerning locking and slip at the interface. Afterward, we spatially and temporally zoom in on a subset of seismic cycles to explore how strain states vary in different segments of the upper plate across seismic cycles. Eventually, the strain cycles in different wedge segments (i.e., outer-wedge, inner-wedge, and coast) are compared to check how similar they respond to the earthquake cycles in a homogeneous wedge with internal discontinuities (i.e., upper plate faults).

3.1 Model Evolution from long to short timescales

3.1.1 Wedge anatomy: Final geometry, surface strain distribution, and structures formed

The cumulative strain pattern maps illustrate the long-term (hundreds of analog earthquake cycle) strain distribution in the upper plate (Figure 6). In the compressional configuration, three different wedge segments are observed: a compressional domain in the outer-wedge, an extensional domain in the inner-wedge, and a compressional domain in the coast. The outer-wedge compressional segment overlies the shallow creeping portion of the interface. Further rearward, the compression domain grades into an extensional domain in the inner-wedge overlying the velocity-weakening zone on the interface at depth. In our experiments, two main mechanisms could cause the permanent extensional strain in the inner-wedge: A minor anelastic component of the mainly elastic coseismic extension and the activity of splay fault-related folds. A compressional segment has also been observed in the coastal area, which may appear on the model's surface as a backthrust fault rooting in the frictional transition zone at the down-dip limit of the velocity weakening zone

(Figures 6).

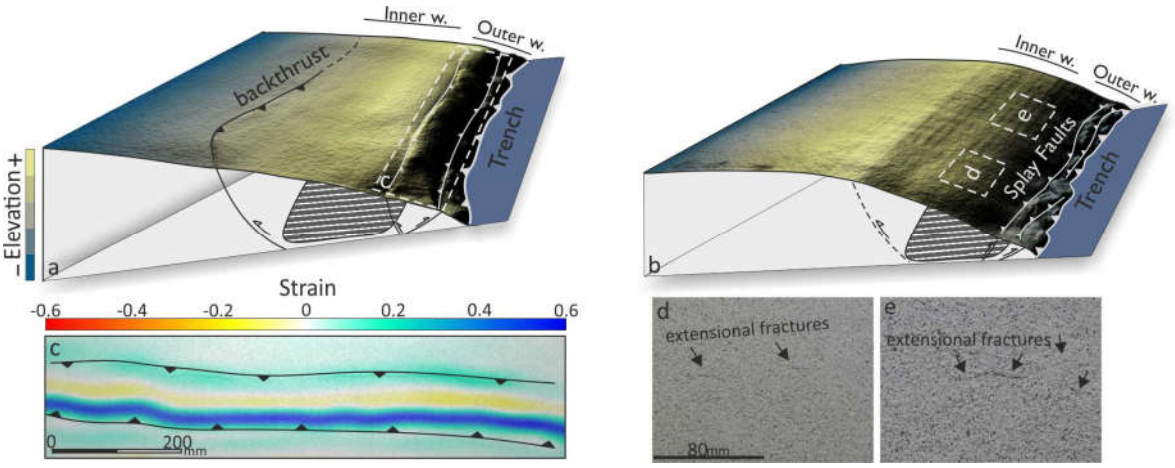

Figure 5: Final surface topography of compressional (a) and extensional (b) configurations. Backthrust and the splay faults are rooted in the down-dip and up-dip limit of the stick-slip zone. The splay faults separate the outer-wedge from the inner-wedge. The strain field generated by the activity of the splay faults is visualized in c. the ridge-shape structure represents extensional strain. Examples of the surface coseismic extensional fracture are shown in d and e.

Localization of deformation has segmented the upper plate into three main segments. The outer-wedge is underthrusted and subsided. The inner-wedge, which is bounded by the up-dip splay fault and downdip backthrust fault, has accumulated the deformation during seismic cycles through internal deformation and vertical displacement due to the activity of the backthrust faults. Further rearward (landward), subsidence occurs in the footwall of the backthrust fault (Figure 6). In the compressional configuration, where the backthrust is developed, the subsiding area is relatively wider (S1).

Both compressional and extensional configurations demonstrate uplift and extension above the seismogenic zone embraced by shortening domains inland and near the trench. However, the compressional domain further rearward (onshore) is smaller in the extensional configuration. Close to the trench, conversely, the upper plate shortens and subsides. In the compressional configuration, the shortening in the transition zone from the shortening domain to the extension domain is accommodated by a pop-up structure forming a conjugated forethrust and backthrust couple. However, the pop-up structure itself generates a local surficial extension domain between

its boundary faults (Figure 5). In the extensional configuration, the forethrusts are the only structures accommodating forearc shortening. In the compressional configuration, the backthrust fault is the main structure accommodating wedge shortening.

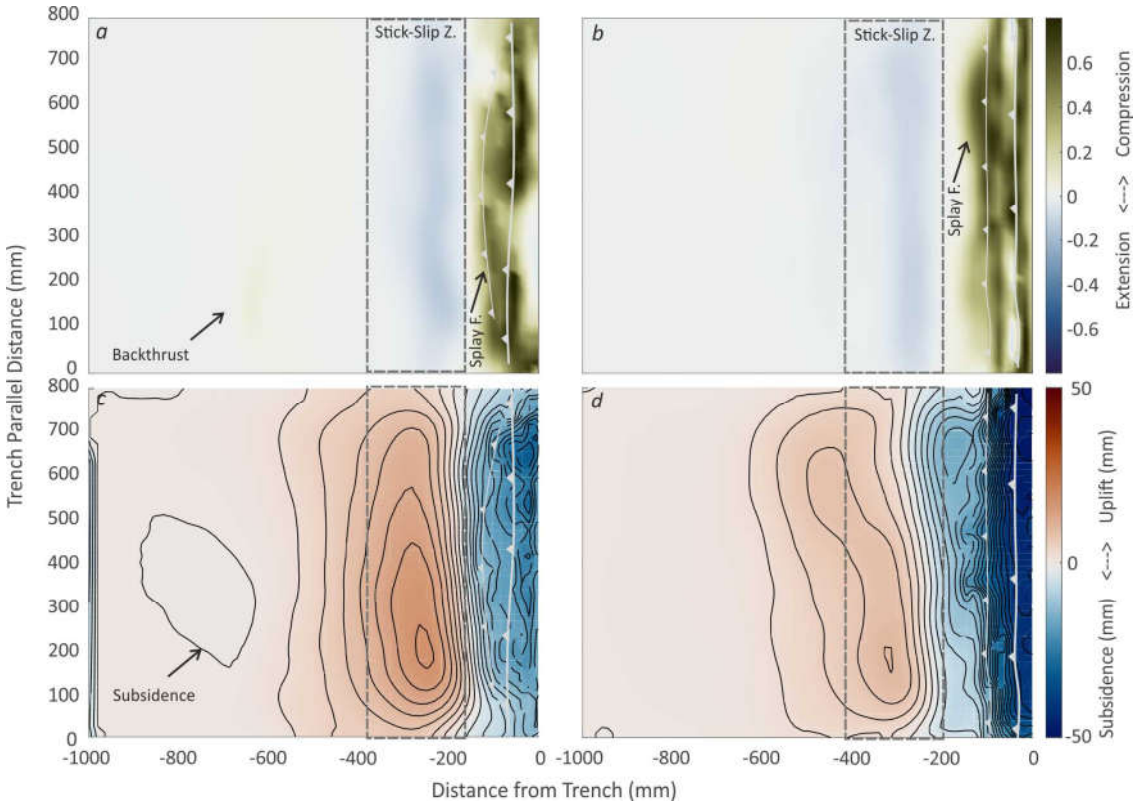

Figure 6: Final surface deformation maps from compressional (a and c) and extensional (b and d) configurations. The approximate location of the stick-slip zone at depth is projected on the model surface as a dashed rectangle. a and b: Surface strain maps from both configurations. Green and blue represent compression and extensional domains, respectively. The outer-wedge is experienced (splay fault and trench domains) compression. Inner-wedge is recorded permanent extension. The activity of the backthrust is evident in the compressional configurations. c and d: permanent vertical deformation in the absence of erosion in the system. The outer- and inner-wedge represent permanent subsidence and uplift, respectively. The slight subsidence zone onshore may represent a forearc basin at the natural scale.

3.1.2 Upper plate faults evolution over time

During model evolution, the first structures appear in the vicinity of the deformation front (near the trench). In the compressional configuration, near the trench, a trenchward-dipping (backthrust) and a rearward-dipping (forethrust) thrust faults form shortly after each other. These two trench-parallel faults, likely conjugate at depth, create a ridge-shaped structure (Figure 3). The structures

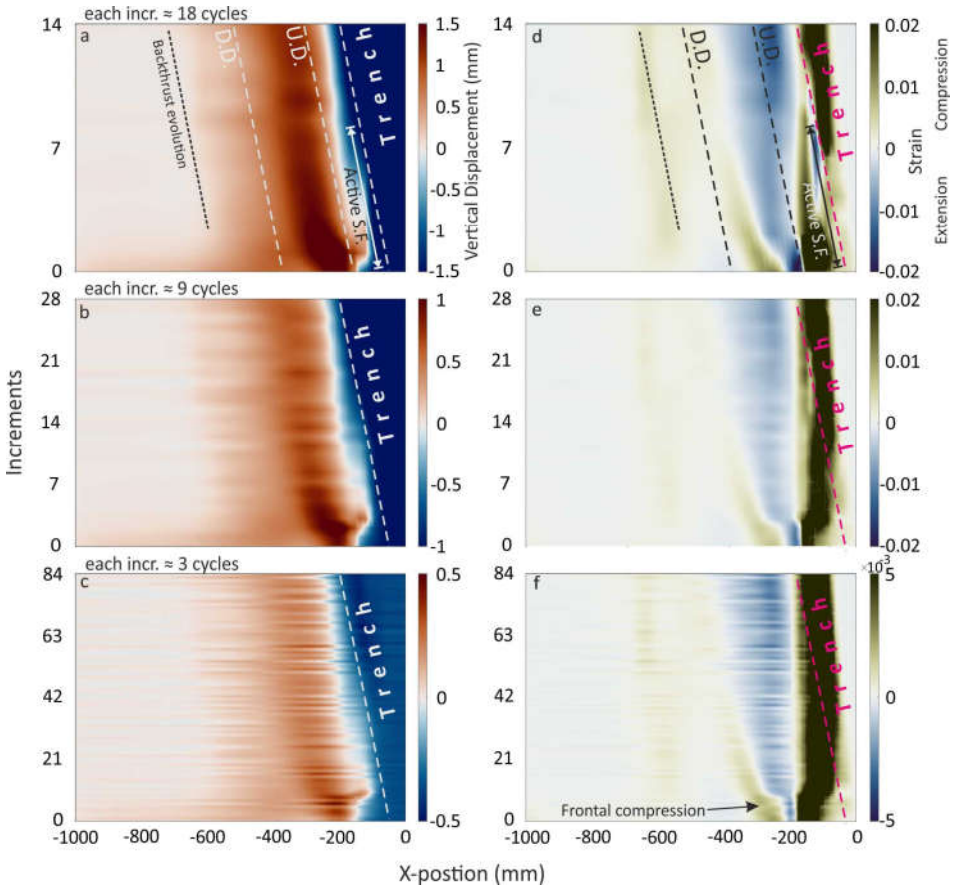

Figure 7: Incremental surface vertical displacement and strain over time from the compressional configuration with different temporal resolutions (3, 9, and 18 analog earthquake cycles). Up-dip (U.D.) and down-dip (D.D.) of the stick-slip zone at depth have been projected on the surface. a-c represents vertical uplift (warm color) and subsidence (cold color). The activity of the splay fault (S.F.) is evident while it is gradually deactivated and the whole slip is transferred on the megathrust. d-f represents surface strain maps with different temporal resolutions.

are formed above the upper basal frictional transition. The stick-slip (seismogenic) zone represents high basal friction in a long-term (interseismic) interval relative to the interface's uppermost portion, which creeps interseismically. This frictional contrast thus leads to a sharp slip rate variation and stress concentrations along the interface where thrusts nucleate. Another active trenchward-dipping thrust fault (backthrust) forms further rearward in the wedge, representing the onshore segment of the forearc. Again, the frictional contrast between the velocity weakening portion of the interface (seismogenic zone) and the downdip limit of this portion controls the origin of the backthrust, thereby accommodating the difference in slip rate (Figures 5 and 6). The thrust

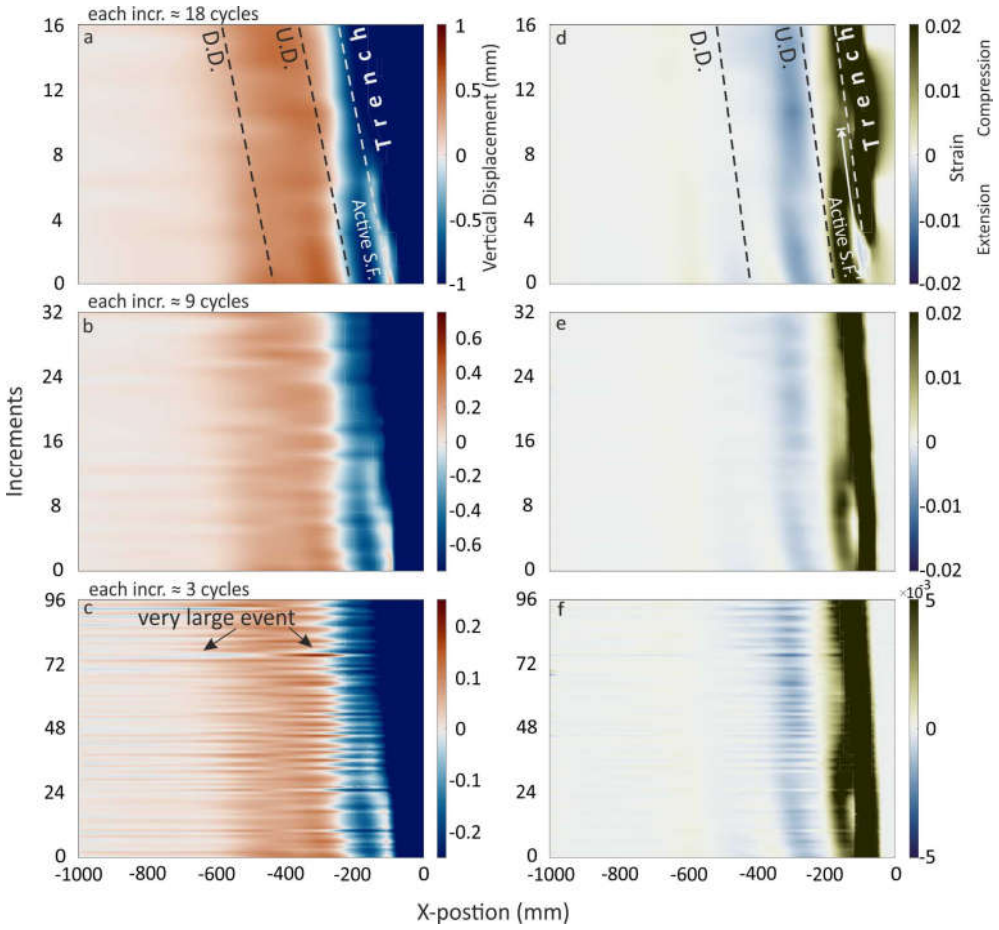

Figure 8: Incremental surface vertical displacement and strain over time from an extensional configuration with different temporal resolutions (3, 9, and 18 analog earthquake cycles). Up-dip (U.D.) and down-dip (D.D.) of the stick-slip zone at depth have been projected on the surface. a-c represents vertical uplift (warm color) and subsidence (cold color). The activity of the splay fault (S.F.) is evident while it is gradually deactivated and the whole slip is transferred on the megathrust. d-f represents surface strain maps with different temporal resolutions.

system accommodates shortening, causing uplift and steepening of the wedge over the course of the experiment consistent with the predicted transiently compressional initial geometry.

In the extensional configuration, a splay forethrust forms at the up-dip limit of the seismogenic zone (Figure 3). In contrast to the compressional wedge, a backthrust does not form at the downdip limit of the seismogenic zone consistent with its stable geometry according to Coulomb wedge theory. These faults show thrust mechanisms and form in the immediate up-dip and down-dip parts of the seismogenic zone.

3.1.3 Long-term wedge deformation: Long-term surface displacement signals reflecting forearc evolution.

To visualize the long-term behavior (i.e., integrating multiple seismic cycles) of the models, forearc wedge differential surface displacement (horizontal and vertical) of increments lasting 150, 75, and 25 seconds are plotted. This covers about 18, 9, and 3 megathrust analog earthquake cycles, respectively (Figures 7 and 8), to illustrate how the wedge evolution is recorded by observational data with different temporal resolutions typical of geomorphological methods (e.g., terrace uplift). In both configurations, the long-term vertical displacement can be temporally divided into two parts depending on whether the upper plate faults are active or inactive. In the case of an active splay fault, the horizontal trenchward displacement terminates at the location of the splay fault (Figure 4), and the zone of maximum uplift is in the hanging-wall of the splay fault (Figures 7 and 8). The splay fault activity decreases over time until it dies, and subsequently, the whole slip is consumed on the interface (i.e., megathrust). Namely, a non-trench-reaching megathrust earthquake system turns into a trench-reaching system over time. The evolution of the backthrust can also be tracked in all temporal resolutions of topography evolution derived from the compressional configuration (Figure 7). The zone of maximum topography correlates with the zone of the maximum extensional segment of the upper plate in both configurations. In the compressional configuration, this extensional zone becomes wider and more pronounced over time, while the width of the zone remains relatively constant over time in the extensional configuration.

Further rearward to the coastal region, the strain evolves differently in the compressional and extensional configurations: In the compressional configuration, the initially extensional strain is replaced by a compressional domain over the entire inner-wedge. The maximum compressional strain appears in the coastal region where the backthrust is formed. The frontal compressional domain diminishes while the compressional wedge is evolving. This is in good agreement with the activity of the up-dip splay fault over its lifetime. The strain pattern over the inner-wedge illustrates that this wedge segment gradually evolves to a more compressional regime. In contrast, there is no significant frontal compressional domain in the extensional configuration (Figure 8), and the inner-wedge is rather in an extensional state. Although the coastal region in the extensional configuration similarly shows a compressional state, the backthrust fault does not appear in the wedge at the down-dip limit of the stick-slip zone.

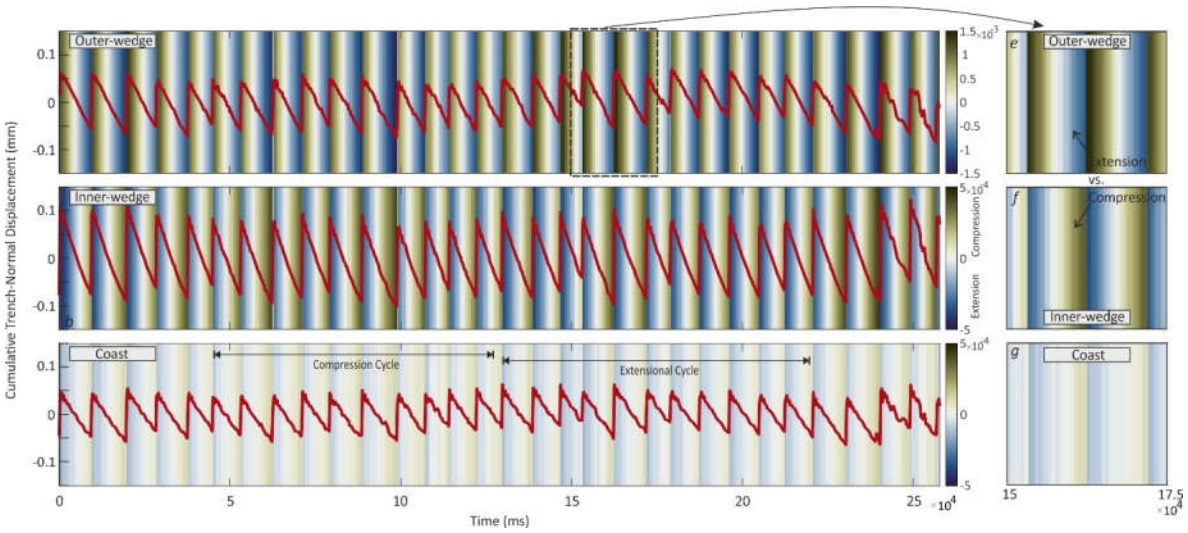

Figure 9: Compressional configuration; Trench-normal displacement time-series (red plot) is overlayed on the strain time-series (background color map) over tens of analog earthquake cycles in different segments of the upper plate. The magnitude of the strain in the outer-wedge is one order larger than the inner-wedge and coast. Note that the outer- and inner-wedge show opposite strain state over the earthquake cycle (compressional versus extensional). The compression and extensional supercycles in the coastal region are shown in the lower panel. Please see the text for the discussion.

3.1.4 Short-term wedge deformation: Strain pattern over seismic cycles

3.1.4.1 Extensional features in the shallow segment of the forearc

The extensional features have generally been observed as extensional fractures or/and crestal normal faults in the frontal wedge domain of the models (Figure 5 and S2). The latter may form above the frictional transition zone at the up-dip limit of the velocity-weakening zone. The activity of the forethrust splay faults plays the main role in their formation being located in the crestal zone in the hanging-wall of the splay fault. This fracture zone reflects the splay fault's activity and, consequently, the up-dip limit (frictional transition) of the velocity-weakening portion of the interface. The extensional features form and develop trench-parallel inelastically over the interseismic interval and are active in opposite modes during the coseismic and postseismic stages, i.e. coseismically extensional and postseimically compressional. The responsible formation mechanism is the splay forethrust the activity of which generates fault-related folds (fault-propagation fold) (S2).

Consequently, a local extensional regime forms at the hinge zone of the fault-related fold and may lead to the crestal normal faults. In the coseismic interval, a sudden slip on the splay fault and megathrust enhances these extensional fractures. The slip on the faults terminates at the frictional

transitional border. Hence, a compressional strain regime appears in the forelimb of the fault-related fold.

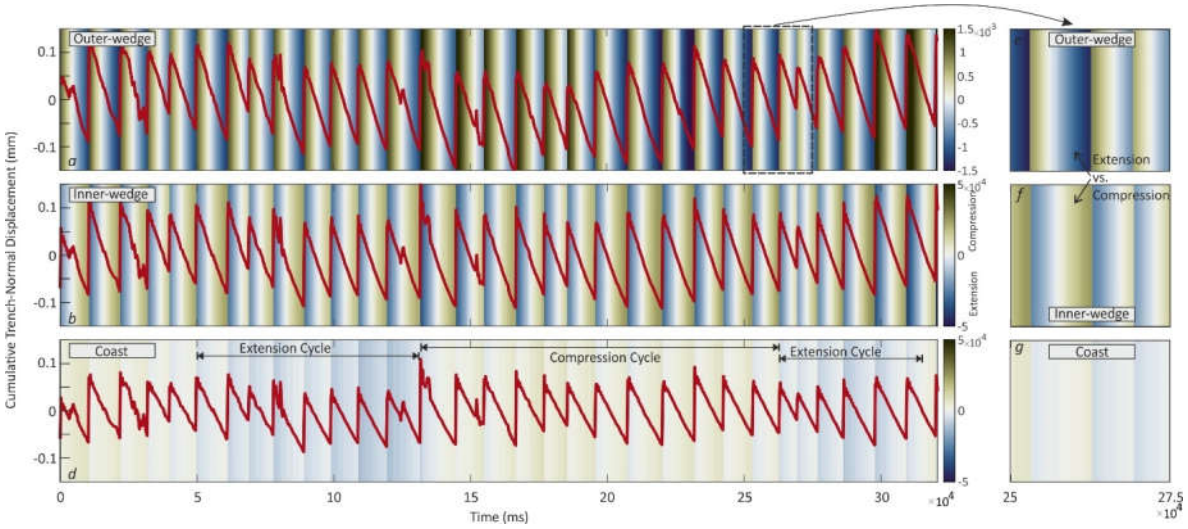

Figure 10: Extensional configuration; Trench-normal displacement time-series (red plot) is overlayed on the strain time-series (background color map) over tens of analog earthquake cycles in different segments of the upper plate. The magnitude of the strain in the outer-wedge is one order larger than the inner-wedge and coast. Note that the outer- and inner-wedge show opposite strain state over the earthquake cycle (compressional versus extensional). The compression and extensional supercycles in the coastal region are shown in the lower panel. Please see the text for the discussion.

The fractures appear in the inner-wedge segment of the model forearc where they overly the velocity-weakening portion of the interface at depth. The extensional fractures in the inner-wedge above the seismogenic zone form coseismically where the maximum extensional strain occurs in the forearc and is partially preserved as anelastic deformation (i.e., normal faulting) in the inner-wedge in each earthquake cycle. In contrast, during the interseismic period, this segment of the forearc is mainly under compression.

3.1.4.2 Strain-state cycle over the seismic cycle

Here we have visualized the average value of the strain over three different segments of the upper plate forearc to take a closer look at the strain evolution at the timescale of individual seismic cycles (Figures 9 and 10). In general, the strain rate reduces rearward from the trench toward the coast, consistent with the dominance of elastic loading at the seismic cycle timescale. The outer-wedge shows strains opposite to those of the coast and inner-wedge (Figures 9 and 10). The inner-

wedge and coast are under compression when the outer-wedge is experiencing extension during the interseismic period—this is a general pattern over many seismic cycles. In each cycle, the inner-wedge undergoes extension coseismically, then gradually moves to a neutral state and finally shifts to a stably compressional state and stays in this regime until the next seismic event occurs. In contrast, the outer-wedge is under compression during the earthquake and subsequently experiences neutral and extensional states in the interseismic interval. In both segments, the strain state shows a regular cycle and follows the same earthquake cycle trend.

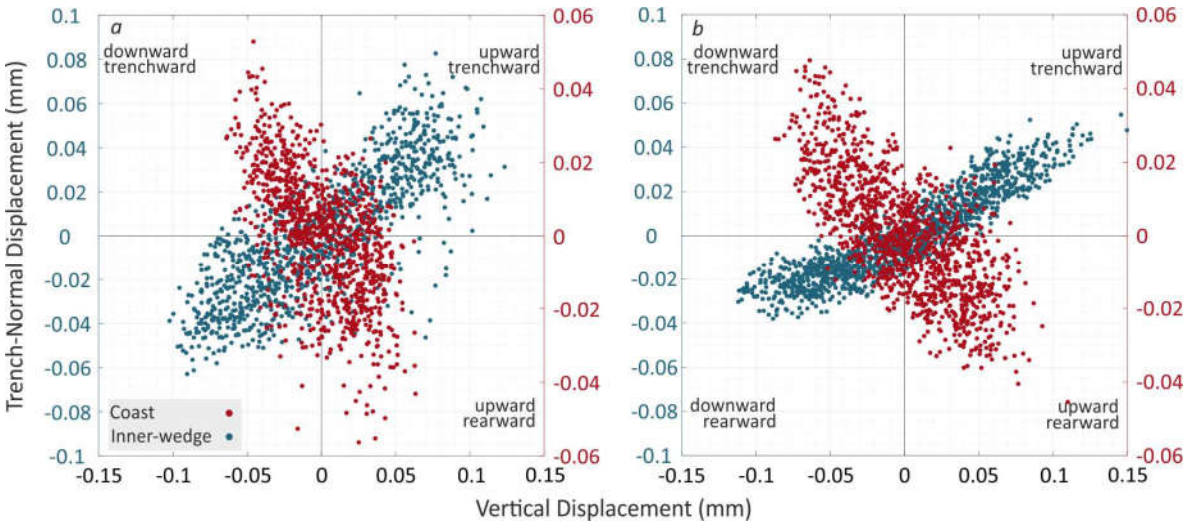

Figure 11: Comparison between surface displacements (horizontal and vertical) in the inner-wedge and coast segments. The segments demonstrate opposite trends: the coast moves trenchward while subsiding (and vice versa), but the inner-wedge moves trenchward while moving upward.

In the down-dip segment, which is treated as underlying the coastal area in our experiment (cf. Fig. 1), the strain state cycle differs from that of the two shallower (offshore) segments of the upper plate. Although the strain magnitude is approximately an order of magnitude smaller, its pattern may be closer to the inner-wedge than to the outer-wedge.

Interestingly, the strain state represents not only an asymmetric cyclic pattern over stick-slip cycles but also a longer cycle (hereafter called “supercycle”) (Figures 9 and 10). In the coastal segment, unlike the other upper plate segments, the extensional and compressional portions of the strain do not balance over a few cycles but show multi-cycle long compressional and extensional supercycles. The supercycle appears sharper in the extensional configuration, where the backthrust is not developed. It may, therefore, be due to the activity of the backthrust that perturbs the

supercycle. The surface displacements in the coastal zone and the inner-wedge represent opposite trends (Figure 11). In the coseismic period, the coast, which overlies the down-dip limit of the stick-slip zone, moves trenchward while subsiding (and vice versa in the interseismic period), but the inner-wedge, which overlies the stick-slip zone, moves trenchward while moving upward. This implies that coseismic uplift and subsidence patterns indicate the location of the slipped zone at depth. The possible primary mechanisms for the supercycle will be discussed in the discussion.

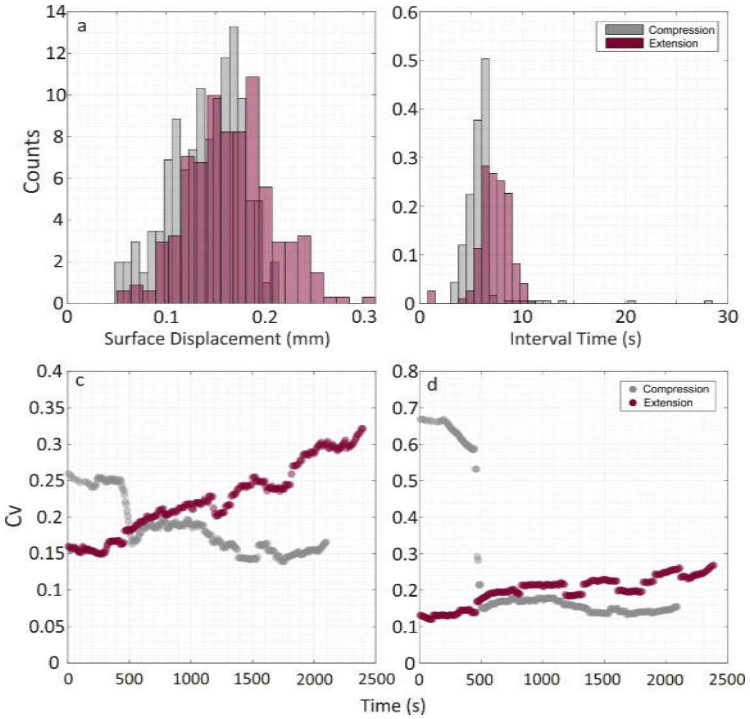

Figure 12 : Size and frequency distributions (a and b) and coefficients of variation (Cv) of recurrence intervals and size (c and d) of analog megathrust events for compressional and extensional configurations.

3.2 Frequency and size distributions of analogue megathrust events

To explore the possible relationship between moment release patterns and forearc configurations, we compare the frequency and size of analog megathrust events and their coefficients of variations (Cv). This coefficient is defined as the ratio of the mean to the standard deviation of the data, from both compressional and extensional configurations (Kuehn et al., 2008; Rosenau & Oncken, 2009). We have defined a moving window to calculate the coefficient of variation over the size and frequency of events. The coefficient of variation generally exhibits an inverse relationship (i.e.,

401 negative correlation) with the periodicity of the frequency-size distribution. In particular, a Cv >
402 0.5 indicates random events while a CV < 0.5 characterizes periodic events.
403 The results of the size and frequency distribution and temporal evolution of the frequency-size
404 distributions are plotted in figure 12. Accordingly, the extensional configuration is characterized
405 by relatively larger event size and longer recurrence. In the Cv plots of the compressional
406 configuration (Figure 12 c and d), a sharp reduction is clear. Its timing shows a good agreement
407 with the evolution of the main upper plate structures (i.e., backthrust fault). The Cv of the
408 compressional configuration is generally lower than that of the extensional configuration,
409 indicating that the first is more periodic. Although both configurations demonstrate rather periodic
410 behavior (i.e. CV<0.5), the recurrence pattern of the extensional configuration, unlike the
411 compressional configuration, evolves over time towards higher variability. The Cv values for the
412 extensional configuration systematically increase and are characterized by a Cv higher than 0.15.
413 In contrast, in the compressional configuration, the values stay in a range of 0.15-0.2. A similar
414 trend is also observed in the size distributions of both models. The compressional configuration
415 does not show a significant evolution over time; however, an increasing trend is observed towards
416 higher coefficients (i.e., less characteristic events over time) in the extensional configuration.
417

418 # 4 Discussion
419
420 ## 4.1 Mechanical state of the shallow forearc over the seismic cycle
421
422 We have used critical wedge theory to design two endmember wedge geometries to see the effect
423 of (transient) instability on the long-term deformation pattern. As shown in figure 2, the wedge is
424 predicted to be critically compressive and stable during the interseismic and coseismic periods,
425 respectively, in the compressional configuration. In the extensional configuration, the onshore and
426 offshore segments of the wedge represent different states: In the coseismic period, the offshore
427 segment, unlike the onshore segment, is prone to be critically extensional. The offshore segment
428 is stable in the interseismic period, but the onshore segment tends to be critically compressional.
429 The outer-wedge segment of our model overlies the creeping portion of the interface where slip
430 instability cannot nucleate but may rupture during trench-reaching megathrust events (Cubas et
431 al., 2013a; Noda and Lapusta, 2013). This domain is near the deformation front and undergoes
432 more deformation and splay thrust faulting than the other forearc segments. This segment switches

its stability state from compressional critical in the interseismic stage to a coseismically stable condition. Analog earthquake studies suggest that a mega-splay fault at the up-dip limit of the velocity-weakening zone may act as a relaxation mechanism for coseismic compression (Rosenau et al., 2009) and be activated in the early postseismic stage of a seismic cycle. These laboratory observations are in good agreement with the aftershock activities after megathrust events, for instance, after the Maule 2010 (Lieser et al., 2014), Antofagasta 1995 (Pastén-Araya et al., 2021), Iquique 2014 (Soto et al., 2019), and Ecuador–south Colombia 1958 earthquakes (J.-Y. Collot et al., 2008; Jean-Yves Collot et al., 2004). This implies that coseismic strengthening of the shallow megathrust pushes the outer-wedge to a compressively critical state during large displacements on the interface (Figure 10) (Hu & Wang, 2008; Wang et al., 2019; Wang & Hu, 2006). Consequently, the splay fault between the outer and inner-wedge may accumulate slip during coseismic or/and postseismic periods.

The inner-wedge is located between this forethrust splay fault and the projection of the down-dip limit of the stick-slip zone to the surface or the backthrust upper-plate fault (Figure 5). This segment is interseismically stable and a minimum of permanent deformation is accumulated (Cubas et al., 2013b). The maximum strain is localized on the backthrust fault which is the landward boundary of the inner-wedge. However, this backthrust may activate with a normal faulting mechanism during or immediately after a large coseismic slip in the velocity-weakening portion of the interface, similar to the activity of the Pichilemu fault shortly after the Maule 2010 megathrust earthquake (Farías et al., 2011; Cubas et al., 2013b). This means that the mechanically most stable segment of the entire wedge – i.e. the inner wedge - reflects the seismically most active (i.e., velocity-weakening) portion of the interface. (Fuller et al., 2006).

4.2 Seismotectonic forearc segmentation: Comparison with natural examples

Our results highlight how coseismic surface deformation may contribute to the morphology of the shallow (offshore) segment of the forearc. The coseismic extension that occurs offshore is mainly observed in the inner-wedge, in the zone bounded by the up-dip forethrust (and/or backthrust) and down-dip backthrust (Figures 5). The up-dip forethrust is the same structure that has been observed in several natural examples. It has been introduced as either backstop in the 2011 Tohoku-Oki earthquake region in the Japan Trench (Ito et al., 2011; Tsuji et al., 2011, 2013) or as the approximate limit between the lower and middle slopes (MLS) in the north Chilean margin (Maksymowicz et al., 2018; Storch et al., 2021). In the former, the fault is characterized by the

boundary between a soft and fractured sediment sequence abutting a less-deformed sequence on the landward side. After the 2011 Tohoku-Oki event, seafloor photographs taken from the splay fault (backstop) region show that extensional steep cliffs are formed coseismically due to small-scale slope failure (Tsuji et al., 2013). We observe similar gravity-induced features in the forelimb of the splay fault in our experiments, indicating the up-dip limit of the coseismic slip on the interface. Further landward, seafloor photographs from the inner-wedge have suggested coseismic anelastic extensional features with no evidence for submarine landslides and reverse faulting as responsible mechanisms (Tsuji et al., 2013). This segment of the upper plate in both our models and the 2011 Tohoku-Oki event overlies the zone of maximum coseismic slip.

Seafloor extensional features have also been documented in the regions of the Maule 2008 and Iquique 2014 earthquakes in the central and northern Chilean subduction zone (Geersen et al., 2016, 2018; Maksymowicz et al., 2018; Reginato et al., 2020; Storch et al., 2021). A normal faulting escarpment and extensional fractures are observed on the hanging wall of the forethrust splay in the Maule 2008 earthquake region (Geersen et al., 2016). Although it is not evident whether the normal faults are rooted in the megathrust interface, the extensional fractures on the hanging wall may be related to the activity of the splay fault. As shown in our model's results, the activity of the splay fault at the up-dip limit of the rupture area may generate an extensional regime in the hinge zone of the fault-related fold and forms extensional fractures. Note that these frontal splay faults may be active during earthquakes and/or in postseismic intervals. In both cases, however, they indicate the frictional transition zone on the plate interface and, in consequence, the up-dip limit of the locked seismogenic zone. In line with our model result, the extensional basin between the splay fault (backstop) and coastal region indicates the megathrust seismogenic zone at depth (Moscoso et al., 2011). The large subduction earthquakes may rupture different portions of the interface from the trench to the downdip end of the seismogenic zone (Lay et al., 2012). Depending on the earthquake magnitude and position of the ruptured segment (i.e., the portion of the megathrust interface beneath the coastal region), the extensional fractures can also be seen onshore as a marker of permanent deformation (Baker et al., 2013; Loveless et al., 2005, 2009).

In the Iquique 2014 earthquake region (North Chilean subduction system), clear evidence of the extensional features in the upper plate has been reported from offshore seismic profiles (Geersen et al., 2018; Reginato et al., 2020; Storch et al., 2021). The offshore extensional features can be categorized into two domains, the Middle-Lower slope transition (MLS), and Middle-Upper slope

segments. The former is likely formed by the activity of the large forethrust splay, which may be active during co-, post-, and interseismic intervals. The Middle-Upper slope segment overlies the main slip zone of the 2014 event. It is possibly formed coseismically and generates the sedimentary basin over hundreds of seismic cycles. This latter correlation also correlates with the gravity anomaly (Schurr et al., 2020) introduced by (Song & Simons, 2003; Wells et al., 2003).

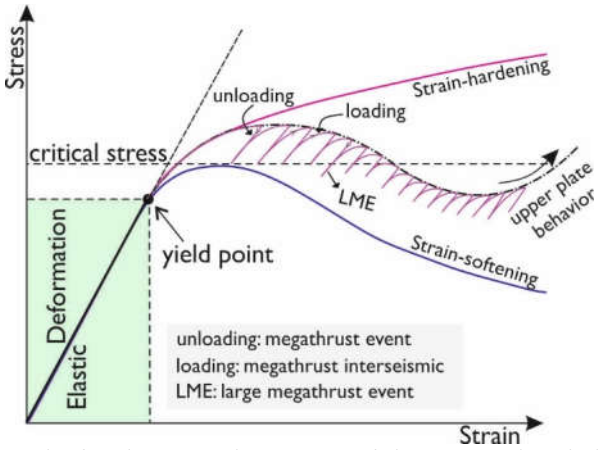

Figure 13: A suggested scenario for the coastal segment of the upper plate behavior over tens of seismic cycles. After exceeding the elastic domain, the upper plate at the location of the coast goes to the strain-hardening domain over a few seismic cycles and then moves towards the strain-softening domain. The pulses of megathrust events (loading and unloading) accelerate this switch from strain-hardening to strain-softening.

4.3 Forearc segmentation and temporal pattern of events

The compressional configuration establishes a clear forearc segmentation through forming up-dip (offshore) splay faults and down-dip (onshore) backthrust faults, causing the analog megathrust events to be more regular (same evolution as in Rosenau and Oncken, 2009). Lacking a backthrust, the extensional wedge does not have this clear segmentation, causing more irregular analog megathrust events. However, both are still generally periodic, i.e. CV<0.5. Moreover, the forearc segment bounded by the upper plate faults overlies the seismogenic zone; hence, the frontal shortening segment (i.e., inner-wedge) of the compressional configuration behaves as a deterministic spring-slider system (Reid, 1910; Rosenau & Oncken, 2009). In the extensional configuration, the extensional fractures on the segment above the seismogenic zone indicate anelastic deformation that correlates with a more complicated temporal pattern of the megathrust events. This is equivalent to the observation of a less periodic pattern of analog earthquakes

produced in the extensional configuration.

4.4 Coastal strain cycle in response to earthquake cycle

In our model, the projection of the downdip limit of the velocity weakening zone on the surface represents the coastal region (Oleskevich et al., 1999; Ruff & Tichelaar, 1996). Unlike the inner-wedge and outer-wedge, the coastal region reacts in an inhomogeneous pattern to the seismic cycles: its strain state does not only respond to each event (i.e., megathrust earthquake), but the strain state shows a "supercycle" over several cycles. In other words, a "strain-switch" from compressional/extensional to an extensional/compressional state develops over a few cycles (Figures 9 and 10). We hypothesize that internal deformation in the experimentally well-known elastoplastic deformation cycle may be the responsible mechanism for the supercycle. The strain rate in the coastal domain is at least one order of magnitude lower than that in the offshore forearc segments; hence, the onshore segment needs more time to reach its yield strength and to shift between strain-hardening and strain-softening periods.

On the other hand, a stress transfer caused by a megathrust earthquake perturbs this process and accelerates/decelerates the deformation rate. When the coastal area is in a strain-hardening period, megathrust coseismic pulses gradually push it toward a neutral stage approaching failure and the resultant switch to strain-softening. However, a very large coseismic pulse may also quickly drag it into the strain-softening domain. After the coseismic event, the coast again moves toward the strain-hardening regime (Figure 13). These changes in the stain cycles reflect variability in strain rate with respect to the long-term trend such that the compressional wedge is more segmented, its deformation varies less compared to the unsegmented extensional wedge.

Observations reveal that a relatively low resolution (18 cycles in this case) may provide a good overview of the wedge evolution type as outlined above. However, the details of the cycles and the transient in between may be overprinted, for example, by the supercycle-related uplift/subsidence and megathrust events involving splay faults. The comparison suggests that the seismic cycle-to-cycle variability causes periodicity in the surface deformation at all (observational) frequencies. The Northwest Coast of the Tohoku-Oki 2011 earthquake (NE Japan; Japan trench) and the Pacific coast of Hokkaido (Kuril trench) have both experienced two different long-term vertical movement histories. In the former case, the Pleistocene marine terrace

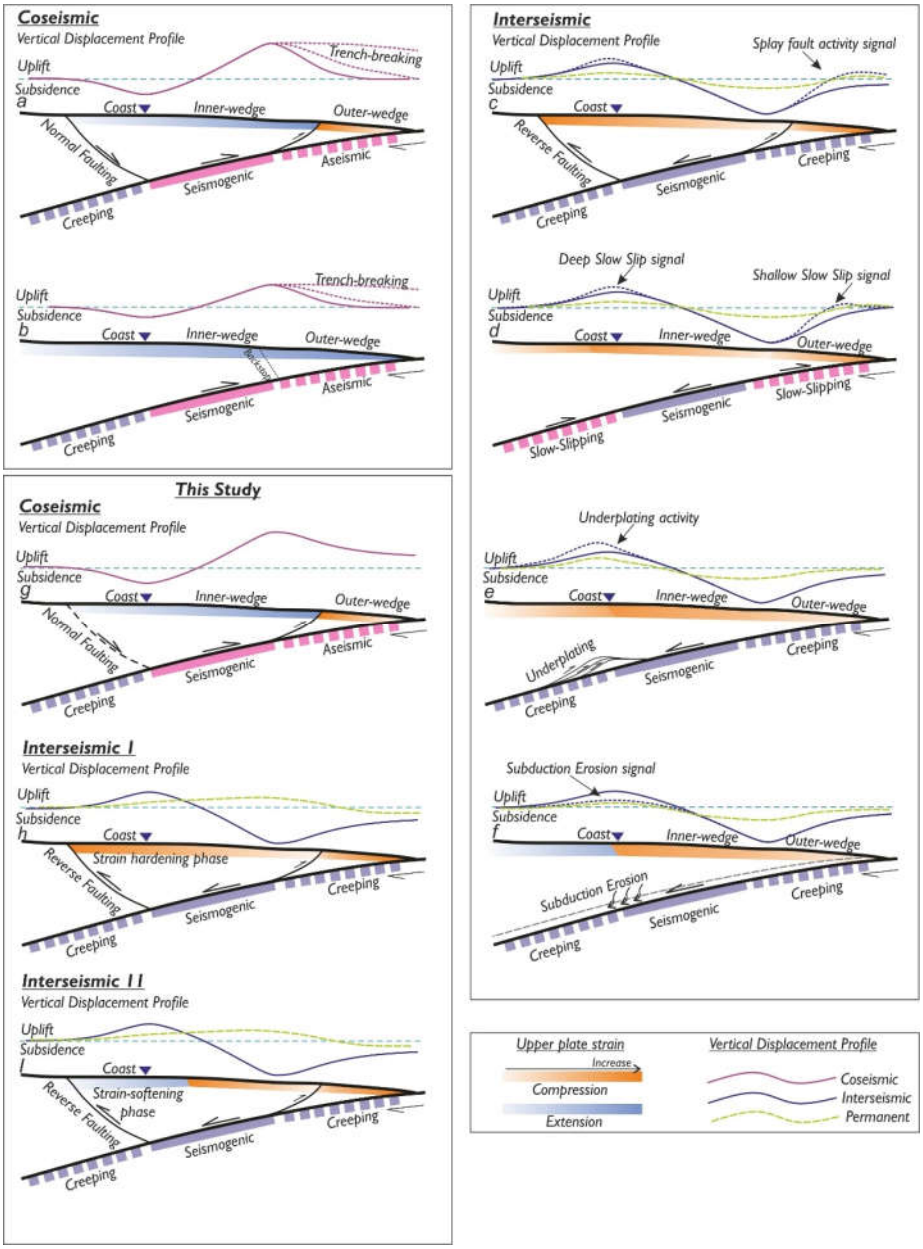

Figure 14: Schematic of vertical displacement and strain state during the coseismic period and interseismic interval in different segments of upper plates for different scenarios. Note that we assume the coast reflects the down-dip limit of the seismogenic zone at depth; modified after (Clark et al., 2019; Farías et al., 2011; Herman & Govers, 2020; Madella & Ehlers, 2021; Melnick et al., 2018; Menant et al., 2020; Moreno et al., 2009; Mouslopoulou et al., 2016; Ozawa et al., 2011; Rosenau & Oncken, 2009; Simons et al., 2011; Sun et al., 2017; Wang et al., 2019; Wang & Tréhu, 2016, and many others).

559 chronology of the NE coast of Japan has experienced a constant uplift at about 0.2 m/ky.
560 (Matsu'ura et al., 2019). In contrast, the Holocene sedimentary succession in the south and central
561 Sanriku suggests subsidence at about 1 mm/yr. (Niwa et al., 2017). If this opposite long-term
562 coastal vertical movement is accurate enough, it may reflect the coastal strain supercycle in
563 response to the megathrust cycle. In the latter case, the sedimentological investigations and diatom
564 assemblages suggest pre-seismic submergence at a rate of 8–9 mm/yr. (Atwater et al., 2016; Sawai,
565 2020; Sawai et al., 2004). If this rapid subsidence occurs in each earthquake cycle, megathrust
566 coseismic and postseismic deformation should generate 4–5 m of coastal uplift in each cycle to
567 cancel out the subsidence. A similar subsidence-uplift pattern also accrued in the Aleutian-Alaska
568 subduction system (Shennan & Hamilton, 2006).
569 The above inconsistency in vertical movement of the coast occurs in subduction systems where
570 the megathrust earthquake usually ruptured the offshore (i.e., shallow) part of the interface (e.g.,
571 Japan and Alaska trenches) (Figure 14). In the cases where the megathrust earthquakes that
572 partially or fully ruptured the deep part of the interface, for instance, the Antofagasta 1995 (Chlieh
573 et al., 2004; Pritchard et al., 2002) and Illapel 2015 earthquakes (Tilmann et al., 2016), marine
574 terraces recorded a more continuous uplift (with different rates) since the Pleistocene (González-
575 Alfaro et al., 2018). However, a long-term (Miocene) change in the vertical movement has been
576 recorded in some places on the Coastal Cordillera in the Chilean margin, probably caused by basal
577 erosion/accretion sequences (Encinas et al., 2012). This may imply that if the coastal area subsides
578 coseismically but uplifts over the interseismic period, the coast probably overlies the downdip
579 limit of the locked zone while the coastal region may show long-term vertical movement
580 inconsistently. If the coast moves vertically upward during both coseismic and interseismic
581 periods, upper plate thrust faults likely push the coast upward (Clark et al., 2019; Mouslopoulou
582 et al., 2016) and the coastal region continuously accumulates permanent uplift.
583 Deep slow-slip events, basal accretion, interseismic crustal thickening, and upper plate faulting
584 may enhance coastal uplift at different time scales (Figure 14). Among these processes,
585 underplating may not play a significant portion in a single seismic cycle because the formation of
586 each tectonic slice (i.e., duplex) is in a Myr-scale (Menant et al., 2020; Ruh, 2020). The thermo-
587 mechanical simulations (Menant et al., 2020) suggest early and late stages of a single underplating
588 cycle respectively characterized by up to 1.5 mm/yr. uplift and subsidence (i.e., re-equilibration of
589 the forearc wedge) rate in the coastal region. This transition from uplift to subsidence (and vice

versa) is in the Myr-scale and represents a much lower frequency in comparison with the deformation supercycle observed in our experiments. However, to rule out and differentiate the impact of the different mechanisms involved in the vertical movement of the coastal region, a modeling approach including all the above-mentioned mechanisms is needed.

Table 1: Summary of short- and long-term forearc strain state

Configuration	**Compressional config.**	**Compressional config.**	**Compressional config.**	**Extensional config.**	**Extensional config.**	**Extensional config.**
Forearc segment	***Coseismic***	***Interseismic***	***Long-term permanent***	***Coseismic***	***Interseismic***	***Long-term permanent***
outer-wedge	Compression	From compression moves to a neutral state and finally to extension	Compression	Compression	From compression moves to a neutral state and finally to extension	Compression
Inner-wedge	Extension	From extension moves to a neutral state and finally to a stably compressional	Extensional; extensional zone becomes wider over time	Extension	From extension moves to a neutral state and finally to a stably compressional	Extensional over the seismogenic zone; surface extentional fractures
Coastal region	Extension	Extensional & compressional portions do not balance; asymmetric cyclic pattern	Multi-cycle long compressional/ extensional supercycles	Extension	Extensional & compressional portions do not balance; asymmetric cyclic pattern	Multi-cycle long compressional/ extensional supercycles; sharper supercycle

Although the inner-wedge and outer-wedge may show a relatively simple earthquake deformation cycle, the coastal zone in the subduction zones may also show a rather complicated pattern and trend. Where the downdip limit of seismic locking and slip is offshore, both, the deformation resulting from seismic cycle deformation and that from mass flux at the plate interface (subduction erosion vs. underplating) generate a composite, more complex kinematic record, even in our simplified seismotectonic model. This implies that predicting the interface behavior from the coastal behavior might not always provide diagnostic evidence in the case of shallow subduction earthquakes where the coast does not overlie the seismogenic zone or its downdip end. Rather, measuring surface deformation above the locked zone provides a more reliable indication of the behavior of the interface.

5 Conclusion

Our results highlight that, in the shallow portion of the subduction zone, frictional properties of the interface and mechanical characteristics of the forearc determine the surface deformation signal over seismic cycles. The mechanical and kinematic interaction between the shallow wedge and the interface can partition the wedge into different segments. These segments may react analogously

or oppositely over the different intervals of the seismic cycle (Table 1). Moreover, different wedge segments may switch their strain state from compression/extension to extension/compression domains. We emphasize that a more segmented upper plate is related to megathrust subduction that generates more characteristic and periodic events.

Our experiments underscore that the stable part of the wedge (i.e., inner-wedge) which undergoes extension coseismically overlies the seismogenic zone. However, the density of extensional fractures and the number of normal faults may increase toward the limit between the inner-wedge and outer-wedge due to the activity of splay faults at the up-dip limit of the seismogenic zone.

Over a dozen and more analog earthquake cycles, the strain time series reveal that the strain state may switch the mode after remaining quasi-stable over a few seismic cycles in the coastal zone. Various scenarios have been suggested, such as background seismicity, deep slow-slip events, subduction accretion/erosion, as the responsible mechanism for switching the kinematic behavior of the coastal domain (uplift to subsidence and vice versa). Here we additionally show that the mechanical state of the plate interface beneath the coastal region, may vary over time and influence the coastal region strain state. Because the strain rate here is significantly lower than in the offshore segment, this may eventually lead to different observed vertical motions on the coast. Megathrust events might be a driving agent that accelerates the strain state switch and pushes the coastal region from a strain-hardening to strain-softening state. Our simplified experiments demonstrate that the strain cycle in the coastal region may show a supercycle pattern superseding sawtooth pattern of the strain cycles related to the earthquake cycle. This is geodetically relevant as the observations in many subduction zones are focused in the coastal regions. Hence, it may not always be straightforward to use these observations as direct evidence to assess the behavior of the shallow, offshore portion of the megathrust.

Data Availability Statement

All data in this study will be published open access soon (data archiving is underway). We thank GFZ Data Services for publishing the data. Meanwhile, the data set is uploaded as Supplemental Material for review purposes.

Acknowledgment

The research is supported by the SUBITOP Marie Sklodowska-Curie Action project from the European Union's EU Framework Programme for Research and Innovation Horizon 2020 (Grant Agreement 674899) and Deutsche Forschungsgemeinschaft (DFG) through Grant CRC 1114 "Scaling Cascades in Complex Systems," Project 235221301 (B01). The authors thank M. Rudolf, F. Neumann, and Th. Ziegenhagen for their helpful discussion and assistance during our laboratory experiments. Some uniform colormaps are adapted from Crameri, (2018).

Refrences

Adam, J., Urai, J. L., Wieneke, B., Oncken, O., Pfeiffer, K., Kukowski, N., Lohrmann, J., Hoth, S., Van Der Zee, W., & Schmatz, J. (2005). Shear localisation and strain distribution during tectonic faulting—New insights from granular-flow experiments and high-resolution optical image correlation techniques. *Journal of Structural Geology*, *27*(2), 283–301.

Atwater, B. F., Furukawa, R., Hemphill-Haley, E., Ikeda, Y., Kashima, K., Kawase, K., Kelsey, H. M., Moore, A. L., Nanayama, F., Nishimura, Y., Odagiri, S., Ota, Y., Park, S.-C., Satake, K., Sawai, Y., & Shimokawa, K. (2016). Seventeenth-century uplift in eastern Hokkaido, Japan: *Http://Dx.Doi.Org/10.1191/0959683604hl726rp*, *14*(4), 487–501. https://doi.org/10.1191/0959683604HL726RP

Baker, A., Allmendinger, R. W., Owen, L. A., & Rech, J. A. (2013). Permanent deformation caused by subduction earthquakes in northern Chile. *Nature Geoscience 2013 6:6*, *6*(6), 492–496. https://doi.org/10.1038/ngeo1789

Caniven, Y., & Dominguez, S. (2021). Validation of a Multilayered Analog Model Integrating Crust-Mantle Visco-Elastic Coupling to Investigate Subduction Megathrust Earthquake Cycle. *Journal of Geophysical Research: Solid Earth*, *126*(2), e2020JB020342. https://doi.org/10.1029/2020JB020342

Chlieh, M., Avouac, J. P., Sieh, K., Natawidjaja, D. H., & Galetzka, J. (2008). Heterogeneous

673 coupling of the Sumatran megathrust constrained by geodetic and paleogeodetic
674 measurements. *Journal of Geophysical Research: Solid Earth*, *113*, 5305.
675 https://doi.org/10.1029/2007JB004981

676 Chlieh, M., De Chabalier, J. B., Ruegg, J. C., Armijo, R., Dmowska, R., Campos, J., & Feigl, K.
677 L. (2004). Crustal deformation and fault slip during the seismic cycle in the North Chile
678 subduction zone, from GPS and InSAR observations. *Geophysical Journal International*,
679 *158*(2), 695–711. https://doi.org/10.1111/J.1365-246X.2004.02326.X

680 Clark, K., Howarth, J., Litchfield, N., Cochran, U., Turnbull, J., Dowling, L., Howell, A.,
681 Berryman, K., & Wolfe, F. (2019). Geological evidence for past large earthquakes and
682 tsunamis along the Hikurangi subduction margin, New Zealand. *Marine Geology*, *412*, 139–
683 172. https://doi.org/10.1016/J.MARGEO.2019.03.004

684 Collot, J.-Y., Agudelo, W., Ribodetti, A., & Marcaillou, B. (2008). Origin of a crustal splay fault
685 and its relation to the seismogenic zone and underplating at the erosional north Ecuador–
686 south Colombia oceanic margin. *Journal of Geophysical Research: Solid Earth*, *113*(B12),
687 12102. https://doi.org/10.1029/2008JB005691

688 Collot, Jean-Yves, Marcaillou, B., Sage, F., Michaud, F., Agudelo, W., Charvis, P., Graindorge,
689 D., Gutscher, M.-A., & Spence, G. (2004). Are rupture zone limits of great subduction
690 earthquakes controlled by upper plate structures? Evidence from multichannel seismic
691 reflection data acquired across the northern Ecuador–southwest Colombia margin. *Journal*
692 *of Geophysical Research: Solid Earth*, *109*(B11), 1–14.
693 https://doi.org/10.1029/2004JB003060

694 Corbi, F., Sandri, L., Bedford, J., Funiciello, F., Brizzi, S., Rosenau, M., & Lallemand, S. (2019).
695 Machine Learning Can Predict the Timing and Size of Analog Earthquakes. *Geophysical*
696 *Research Letters*, *46*(3), 1303–1311. https://doi.org/10.1029/2018GL081251

697 Corbi, Fabio, Bedford, J., Sandri, L., Funiciello, F., Gualandi, A., & Rosenau, M. (2020).
698 Predicting imminence of analog megathrust earthquakes with Machine Learning:
699 Implications for monitoring subduction zones. *Geophysical Research Letters*, *47*(7),
700 e2019GL086615. https://doi.org/10.1029/2019GL086615

Corbi, Fabio, Herrendörfer, R., Funiciello, F., & van Dinther, Y. (2017). Controls of seismogenic zone width and subduction velocity on interplate seismicity: Insights from analog and numerical models. *Geophysical Research Letters*, *44*(12), 6082–6091. https://doi.org/10.1002/2016GL072415

Crameri, F. (2018). *Scientific colour-maps*. https://doi.org/10.5281/ZENODO.1287763

Cubas, N., Avouac, J. P., Leroy, Y. M., & Pons, A. (2013a). Low friction along the high slip patch of the 2011 Mw 9.0 Tohoku-Oki earthquake required from the wedge structure and extensional splay faults. *Geophysical Research Letters*, *40*(16), 4231–4237. https://doi.org/10.1002/grl.50682

Cubas, Nadaya, Avouac, J. P., Souloumiac, P., & Leroy, Y. (2013b). Megathrust friction determined from mechanical analysis of the forearc in the Maule earthquake area. *Earth and Planetary Science Letters*, *381*, 92–103. https://doi.org/10.1016/j.epsl.2013.07.037

Cubas, Nadaya, Souloumiac, P., & Singh, S. C. (2016). Relationship link between landward vergence in accretionary prisms and tsunami generation. *GEOLOGY*, *44*. https://doi.org/10.1130/G38019.1

Dahlen, F. A., Suppe, J., & Davis, D. (1984). Mechanics of fold-and-thrust belts and accretionary wedges: Cohesive Coulomb Theory. *Journal of Geophysical Research: Solid Earth*, *89*(B12), 10087–10101. https://doi.org/10.1029/JB089IB12P10087

Delano, J. E., Amos, C. B., Loveless, J. P., Rittenour, T. M., Sherrod, B. L., & Lynch, E. M. (2017). Influence of the megathrust earthquake cycle on upper-plate deformation in the Cascadia forearc of Washington State, USA. *Geology*, *45*(11), 1051–1054. https://doi.org/10.1130/G39070.1

Encinas, A., Finger, K. L., Buatois, L. A., & Peterson, D. E. (2012). Major forearc subsidence and deep-marine Miocene sedimentation in the present Coastal Cordillera and Longitudinal Depression of south-central Chile (38°30′S–41°45′S). *GSA Bulletin*, *124*(7–8), 1262–1277. https://doi.org/10.1130/B30567.1

Farías, M., Comte, D., Roecker, S., Carrizo, D., & Pardo, M. (2011). Crustal extensional faulting triggered by the 2010 Chilean earthquake: The Pichilemu Seismic Sequence. *Tectonics*,

729 *30*(6). https://doi.org/10.1029/2011TC002888

730 Fuller, C. W., Willett, S. D., & Brandon, M. T. (2006). Formation of forearc basins and their
731 influence on subduction zone earthquakes. *Geology*, *34*(2), 65–68.
732 https://doi.org/10.1130/G21828.1

733 Geersen, J., Ranero, C. R., Kopp, H., Behrmann, J. H., Lange, D., Klaucke, I., Barrientos, S.,
734 Diaz-Naveas, J., Barckhausen, U., & Reichert, C. (2018). Does permanent extensional
735 deformation in lower forearc slopes indicate shallow plate-boundary rupture? *Earth and*
736 *Planetary Science Letters*, *489*, 17–27. https://doi.org/10.1016/j.epsl.2018.02.030

737 Geersen, J., Scholz, F., Linke, P., Schmidt, M., Lange, D., Behrmann, J. H., Völker, D., &
738 Hensen, C. (2016). Fault zone controlled seafloor methane seepage in the rupture area of the
739 2010 Maule earthquake, Central Chile. *Geochemistry, Geophysics, Geosystems*, *17*(11),
740 4802–4813. https://doi.org/10.1002/2016GC006498

741 González-Alfaro, J., Vargas, G., Ortlieb, L., González, G., Ruiz, S., Báez, J. C., Mandeng-Yogo,
742 M., Caquineau, S., Álvarez, G., del Campo, F., & del Río, I. (2018). Abrupt increase in the
743 coastal uplift and earthquake rate since ∼40 ka at the northern Chile seismic gap in the
744 Central Andes. *Earth and Planetary Science Letters*, *502*, 32–45.
745 https://doi.org/10.1016/J.EPSL.2018.08.043

746 Herman, M. W., & Govers, R. (2020). Stress evolution during the megathrust earthquake cycle
747 and its role in triggering extensional deformation in subduction zones. *Earth and Planetary*
748 *Science Letters*, *544*, 116379. https://doi.org/10.1016/J.EPSL.2020.116379

749 Hu, Y., & Wang, K. (2008). Coseismic strengthening of the shallow portion of the subduction
750 fault and its effects on wedge taper. *Journal of Geophysical Research: Solid Earth*,
751 *113*(B12), 12411. https://doi.org/10.1029/2008JB005724

752 Ito, Y., Tsuji, T., Osada, Y., Kido, M., Inazu, D., Hayashi, Y., Tsushima, H., Hino, R., &
753 Fujimoto, H. (2011). Frontal wedge deformation near the source region of the 2011
754 Tohoku-Oki earthquake. *Geophysical Research Letters*, *38*(7).
755 https://doi.org/10.1029/2011GL048355

756 Jara-Muñoz, J., Melnick, D., Brill, D., & Strecker, M. R. (2015). Segmentation of the 2010

Maule Chile earthquake rupture from a joint analysis of uplifted marine terraces and seismic-cycle deformation patterns. *Quaternary Science Reviews*, *113*(1), 171–192. https://doi.org/10.1016/J.QUASCIREV.2015.01.005

King Hubbert, M. (1937). Theory of scale models as applied to the study of geologic structures. *Bulletin of the Geological Society of America*, *48*(10), 1459–1520. https://doi.org/10.1130/GSAB-48-1459

Kopp, H. (2013). Invited review paper: The control of subduction zone structural complexity and geometry on margin segmentation and seismicity. *Tectonophysics*, *589*, 1–16. https://doi.org/10.1016/J.TECTO.2012.12.037

Kosari, E., Rosenau, M., Bedford, J., Rudolf, M., & Oncken, O. (2020). On the Relationship Between Offshore Geodetic Coverage and Slip Model Uncertainty: Analog Megathrust Earthquake Case Studies. *Geophysical Research Letters*, *47*(15). https://doi.org/10.1029/2020GL088266

Kuehn, N. M., Hainzl, S., & Scherbaum, F. (2008). Non-Poissonian earthquake occurrence in coupled stress release models and its effect on seismic hazard. *Geophysical Journal International*, *174*(2), 649–658. https://doi.org/10.1111/J.1365-246X.2008.03835.X

Lay, T., Kanamori, H., Ammon, C. J., Koper, K. D., Hutko, A. R., Ye, L., Yue, H., & Rushing, T. M. (2012). Depth-varying rupture properties of subduction zone megathrust faults. *Journal of Geophysical Research: Solid Earth*, *117*(4). https://doi.org/10.1029/2011JB009133

Lieser, K., Grevemeyer, I., Lange, D., Flueh, E., Tilmann, F., & Contreras-Reyes, E. (2014). Splay fault activity revealed by aftershocks of the 2010 Mw 8.8 Maule earthquake, central Chile. *Geology*, *42*(9), 823–826. https://doi.org/10.1130/G35848.1

Loveless, J. P., Allmendinger, R. W., Pritchard, M. E., Garroway, J. L., & González, G. (2009). Surface cracks record long-term seismic segmentation of the Andean margin. *Geology*, *37*(1), 23–26. https://doi.org/10.1130/G25170A.1

Loveless, J. P., Allmendinger, R. W., Pritchard, M. E., & González, G. (2010). Normal and reverse faulting driven by the subduction zone earthquake cycle in the northern Chilean fore

785 arc. *Tectonics*, *29*(2). https://doi.org/10.1029/2009TC002465

786 Loveless, J. P., Hoke, G. D., Allmendinger, R. W., González, G., Isacks, B. L., & Carrizo, D. A.
787 (2005). Pervasive cracking of the northern Chilean Coastal Cordillera: New evidence for
788 forearc extension. *Geology*, *33*(12), 973–976. https://doi.org/10.1130/G22004.1

789 Loveless, J. P., & Meade, B. J. (2011). Spatial correlation of interseismic coupling and coseismic
790 rupture extent of the 2011 MW= 9.0 Tohoku-oki earthquake. *Geophysical Research Letters*,
791 *38*(17). https://doi.org/10.1029/2011GL048561

792 Madella, A., & Ehlers, T. A. (2021). Contribution of background seismicity to forearc uplift.
793 *Nature Geoscience 2021*, 1–6. https://doi.org/10.1038/s41561-021-00779-0

794 Maksymowicz, A., Ruiz, J., Vera, E., Contreras-Reyes, E., Ruiz, S., Arraigada, C., Bonvalot, S.,
795 & Bascuñan, S. (2018). Heterogeneous structure of the Northern Chile marine forearc and
796 its implications for megathrust earthquakes. *Geophysical Journal International*, *215*(2),
797 1080–1097. https://doi.org/10.1093/gji/ggy325

798 Malatesta, L. C., Bruhat, L., Finnegan, N. J., & Olive, J.-A. L. (2021). Co-location of the
799 Downdip End of Seismic Coupling and the Continental Shelf Break. *Journal of*
800 *Geophysical Research: Solid Earth*, *126*(1), e2020JB019589.
801 https://doi.org/10.1029/2020JB019589

802 Matsu'ura, T., Komatsubara, J., & Wu, C. (2019). Accurate determination of the Pleistocene
803 uplift rate of the NE Japan forearc from the buried MIS 5e marine terrace shoreline angle.
804 *Quaternary Science Reviews*, *212*, 45–68.
805 https://doi.org/10.1016/J.QUASCIREV.2019.03.007

806 McCaffrey, R., King, R. W., Payne, S. J., & Lancaster, M. (2013). Active tectonics of
807 northwestern U.S. inferred from GPS-derived surface velocities. *Journal of Geophysical*
808 *Research: Solid Earth*, *118*(2), 709–723. https://doi.org/10.1029/2012JB009473

809 Melnick, D., Bookhagen, B., Strecker, M. R., & Echtler, H. P. (2009). Segmentation of
810 megathrust rupture zones from fore-arc deformation patterns over hundreds to millions of
811 years, Arauco peninsula, Chile. *Journal of Geophysical Research: Solid Earth*, *114*(B1),
812 1407. https://doi.org/10.1029/2008JB005788

Melnick, D., Li, S., Moreno, M., Cisternas, M., Jara-Muñoz, J., Wesson, R., Nelson, A., Báez, J. C., & Deng, Z. (2018). Back to full interseismic plate locking decades after the giant 1960 Chile earthquake. *Nature Communications 2018 9:1*, *9*(1), 1–10. https://doi.org/10.1038/s41467-018-05989-6

Menant, A., Angiboust, S., Gerya, T., Lacassin, R., Simoes, M., & Grandin, R. (2020). Transient stripping of subducting slabs controls periodic forearc uplift. *Nature Communications 2020 11:1*, *11*(1), 1–10. https://doi.org/10.1038/s41467-020-15580-7

Métois, M., Socquet, A., Vigny, C., Carrizo, D., Peyrat, S., Delorme, A., Maureira, E., Valderas-Bermejo, M.-C., & Ortega, I. (2013). Revisiting the North Chile seismic gap segmentation using GPS-derived interseismic coupling. *Geophysical Journal International*, *194*(3), 1283–1294. https://doi.org/10.1093/GJI/GGT183

Molina, D., Tassara, A., Abarca, R., Melnick, D., & Madella, A. (2021). Frictional Segmentation of the Chilean Megathrust From a Multivariate Analysis of Geophysical, Geological, and Geodetic Data. *Journal of Geophysical Research: Solid Earth*, *126*(6), e2020JB020647. https://doi.org/10.1029/2020JB020647

Moreno, M., Rosenau, M., & Oncken, O. (2010). 2010 Maule earthquake slip correlates with pre-seismic locking of Andean subduction zone. *Nature 2010 467:7312*, *467*(7312), 198–202. https://doi.org/10.1038/nature09349

Moreno, M. S., Bolte, J., Klotz, J., & Melnick, D. (2009). Impact of megathrust geometry on inversion of coseismic slip from geodetic data: Application to the 1960 Chile earthquake. *Geophysical Research Letters*, *36*(16), 16310. https://doi.org/10.1029/2009GL039276

Moscoso, E., Grevemeyer, I., Contreras-Reyes, E., Flueh, E. R., Dzierma, Y., Rabbel, W., & Thorwart, M. (2011). Revealing the deep structure and rupture plane of the 2010 Maule, Chile earthquake (Mw = 8.8) using wide angle seismic data. *Earth and Planetary Science Letters*, *307*(1–2), 147–155. https://doi.org/10.1016/J.EPSL.2011.04.025

Mouslopoulou, V., Oncken, O., Hainzl, S., & Nicol, A. (2016). Uplift rate transients at subduction margins due to earthquake clustering. *Tectonics*, *35*(10), 2370–2384. https://doi.org/10.1002/2016TC004248

Niwa, Y., Sugai, T., Matsushima, Y., & Toda, S. (2017). Subsidence along the central to southern Sanriku coast, northeast Japan, near the source region of the 2011 Tohoku-oki earthquake, estimated from the Holocene sedimentary succession along a ria coast. *Quaternary International*, *456*, 1–16. https://doi.org/10.1016/J.QUAINT.2017.08.008

Noda, H., & Lapusta, N. (2013). Stable creeping fault segments can become destructive as a result of dynamic weakening. *Nature 2013 493:7433*, *493*(7433), 518–521. https://doi.org/10.1038/nature11703

Normand, R., Simpson, G., Herman, F., Haque Biswas, R., Bahroudi, A., & Schneider, B. (2019). Dating and morpho-stratigraphy of uplifted marine terraces in the Makran subduction zone (Iran). *Earth Surface Dynamics*, *7*(1), 321–344. https://doi.org/10.5194/ESURF-7-321-2019

Oleskevich, D. A., Hyndman, R. D., & Wang, K. (1999). The updip and downdip limits to great subduction earthquakes: Thermal and structural models of Cascadia, south Alaska, SW Japan, and Chile. *Journal of Geophysical Research: Solid Earth*, *104*(B7), 14965–14991. https://doi.org/10.1029/1999JB900060

Ott, R. F., Gallen, S. F., Wegmann, K. W., Biswas, R. H., Herman, F., & Willett, S. D. (2019). Pleistocene terrace formation, Quaternary rock uplift rates and geodynamics of the Hellenic Subduction Zone revealed from dating of paleoshorelines on Crete, Greece. *Earth and Planetary Science Letters*, *525*, 115757. https://doi.org/10.1016/J.EPSL.2019.115757

Ozawa, S., Nishimura, T., Suito, H., Kobayashi, T., Tobita, M., & Imakiire, T. (2011). Coseismic and postseismic slip of the 2011 magnitude-9 Tohoku-Oki earthquake. *Nature*, *475*(7356), 373–377. https://doi.org/10.1038/nature10227

Pastén-Araya, F., Potin, B., Ruiz, S., Zerbst, L., Aden-Antoniów, F., Azúa, K., Rivera, E., Rietbrock, A., Salazar, P., & Fuenzalida, A. (2021). Seismicity in the upper plate of the Northern Chilean offshore forearc: Evidence of splay fault south of the Mejillones Peninsula. *Tectonophysics*, *800*, 228706. https://doi.org/10.1016/j.tecto.2020.228706

Pritchard, M. E., Simons, M., Rosen, P. A., Hensley, S., & Webb, F. H. (2002). Co-seismic slip from the 1995 July 30 Mw= 8.1 Antofagasta, Chile, earthquake as constrained by InSAR

and GPS observations. *Geophysical Journal International*, *150*(2), 362–376. https://doi.org/10.1046/J.1365-246X.2002.01661.X

Reginato, G., Vera, E., Contreras-Reyes, E., Tréhu, A. M., Maksymowicz, A., Bello-González, J. P., & González, F. (2020). Seismic structure and tectonics of the continental wedge overlying the source region of the Iquique Mw8.1 2014 earthquake. *Tectonophysics*, *796*, 228629. https://doi.org/10.1016/j.tecto.2020.228629

Reid, H. F. (1910). The mechanism of the earthquake, the california earthquake of April 18, 1906, Report of the state earthquake investigation commission. In *Washington DC: Carnegie Institution* (Vol. 2).

Rosenau, M., Corbi, F., & Dominguez, S. (2017). Analogue earthquakes and seismic cycles: Experimental modelling across timescales. *Solid Earth*, *8*(3), 597–635. https://doi.org/10.5194/SE-8-597-2017

Rosenau, M., Horenko, I., Corbi, F., Rudolf, M., Kornhuber, R., & Oncken, O. (2019). Synchronization of Great Subduction Megathrust Earthquakes: Insights From Scale Model Analysis. *Journal of Geophysical Research: Solid Earth*, *124*(4), 3646–3661. https://doi.org/10.1029/2018JB016597

Rosenau, M., Lohrmann, J., & Oncken, O. (2009). Shocks in a box: An analogue model of subduction earthquake cycles with application to seismotectonic forearc evolution. *Journal of Geophysical Research: Solid Earth*, *114*(B1), 1409. https://doi.org/10.1029/2008JB005665

Rosenau, M., Nerlich, R., Brune, S., & Oncken, O. (2010). Experimental insights into the scaling and variability of local tsunamis triggered by giant subduction megathrust earthquakes. *Journal of Geophysical Research: Solid Earth*, *115*(9). https://doi.org/10.1029/2009JB007100

Rosenau, M., & Oncken, O. (2009). Fore-arc deformation controls frequency-size distribution of megathrust earthquakes in subduction zones. *Journal of Geophysical Research*, *114*(B10), B10311. https://doi.org/10.1029/2009JB006359

Ruff, L. J., & Tichelaar, B. W. (1996). What Controls the Seismogenic Plate Interface in

Subduction Zones? *Geophysical Monograph Series*, *96*, 105–111. https://doi.org/10.1029/GM096P0105

Ruh, J. B. (2020). Numerical modeling of tectonic underplating in accretionary wedge systems. *Geosphere*, *16*(6), 1385–1407. https://doi.org/10.1130/GES02273.1

Saillard, M., Audin, L., Rousset, B., Avouac, J.-P., Chlieh, M., Hall, S. R., Husson, L., & Farber, D. L. (2017). From the seismic cycle to long-term deformation: linking seismic coupling and Quaternary coastal geomorphology along the Andean megathrust. *Tectonics*, *36*(2), 241–256. https://doi.org/10.1002/2016TC004156

Sawai, Y. (2020). Subduction zone paleoseismology along the Pacific coast of northeast Japan — progress and remaining problems. *Earth-Science Reviews*, *208*, 103261. https://doi.org/10.1016/J.EARSCIREV.2020.103261

Sawai, Y., Satake, K., Kamataki, T., Nasu, H., Shishikura, M., Atwater, B. F., Horton, B. P., Kelsey, H. M., Nagumo, T., & Yamaguchi, M. (2004). Transient Uplift After a 17th-Century Earthquake Along the Kuril Subduction Zone. *Science*, *306*(5703), 1918–1920. https://doi.org/10.1126/SCIENCE.1104895

Schmalzle, G. M., McCaffrey, R., & Creager, K. C. (2014). Central Cascadia subduction zone creep. *Geochemistry, Geophysics, Geosystems*, *15*(4), 1515–1532. https://doi.org/10.1002/2013GC005172

Schurr, B., Moreno, M., Tréhu, A. M., Bedford, J., Kummerow, J., Li, S., & Oncken, O. (2020). Forming a Mogi Doughnut in the Years Prior to and Immediately Before the 2014 M8.1 Iquique, Northern Chile, Earthquake. *Geophysical Research Letters*, *47*(16), e2020GL088351. https://doi.org/10.1029/2020GL088351

Shennan, I., & Hamilton, S. (2006). Coseismic and pre-seismic subsidence associated with great earthquakes in Alaska. *Quaternary Science Reviews*, *25*(1–2), 1–8. https://doi.org/10.1016/J.QUASCIREV.2005.09.002

Simons, M., Minson, S. E., Sladen, A., Ortega, F., Jiang, J., Owen, S. E., Meng, L., Ampuero, J.-P., Wei, S., Chu, R., Helmberger, D. V., Kanamori, H., Hetland, E., Moore, A. W., & Webb, F. H. (2011). The 2011 Magnitude 9.0 Tohoku-Oki Earthquake: Mosaicking the

925 Megathrust from Seconds to Centuries. *Science*, *332*(6036), 1421–1425.
926 https://doi.org/10.1126/SCIENCE.1206731

927 Song, T. R. A., & Simons, M. (2003). Large trench-parallel gravity variations predict
928 seismogenic behavior in subduction zones. *Science*, *301*(5633), 630–633.
929 https://doi.org/10.1126/science.1085557

930 Soto, H., Sippl, C., Schurr, B., Kummerow, J., Asch, G., Tilmann, F., Comte, D., Ruiz, S., &
931 Oncken, O. (2019). Probing the Northern Chile Megathrust With Seismicity: The 2014
932 M8.1 Iquique Earthquake Sequence. *Journal of Geophysical Research: Solid Earth*,
933 *124*(12), 12935–12954. https://doi.org/10.1029/2019JB017794

934 Storch, I., Buske, S., Victor, P., & Oncken, O. (2021). Seismic images of the Northern Chilean
935 subduction zone at 19°40′S, prior to the 2014 Iquique earthquake. *Geophysical Journal*
936 *International*, *225*(2), 1048–1061. https://doi.org/10.1093/gji/ggab035

937 Sun, T., Wang, K., Fujiwara, T., Kodaira, S., & He, J. (2017). Large fault slip peaking at trench
938 in the 2011 Tohoku-oki earthquake. *Nature Communications*, *8*(1), 1–8.
939 https://doi.org/10.1038/ncomms14044

940 Tilmann, F., Zhang, Y., Moreno, M., Saul, J., Eckelmann, F., Palo, M., Deng, Z., Babeyko, A.,
941 Chen, K., Baez, J. C., Schurr, B., Wang, R., & Dahm, T. (2016). The 2015 Illapel
942 earthquake, central Chile: A type case for a characteristic earthquake? *Geophysical*
943 *Research Letters*, *43*(2), 574–583. https://doi.org/10.1002/2015GL066963

944 Tsuji, T., Ito, Y., Kido, M., Osada, Y., Fujimoto, H., Ashi, J., Kinoshita, M., & Matsuoka, T.
945 (2011). Potential tsunamigenic faults of the 2011 off the Pacific coast of Tohoku
946 Earthquake. *Earth, Planets and Space 2011 63:7*, *63*(7), 831–834.
947 https://doi.org/10.5047/EPS.2011.05.028

948 Tsuji, T., Kawamura, K., Kanamatsu, T., Kasaya, T., Fujikura, K., Ito, Y., Tsuru, T., &
949 Kinoshita, M. (2013). Extension of continental crust by anelastic deformation during the
950 2011 Tohoku-oki earthquake: The role of extensional faulting in the generation of a great
951 tsunami. *Earth and Planetary Science Letters*, *364*, 44–58.
952 https://doi.org/10.1016/j.epsl.2012.12.038

953 Wallace, L. M., Barnes, P., Beavan, J., Dissen, R. Van, Litchfield, N., Mountjoy, J., Langridge,
954 R., Lamarche, G., & Pondard, N. (2012). The kinematics of a transition from subduction to
955 strike-slip: An example from the central New Zealand plate boundary. *Journal of*
956 *Geophysical Research: Solid Earth*, *117*(B2), 2405. https://doi.org/10.1029/2011JB008640

957 Wang, K., Brown, L., Hu, Y., Yoshida, K., He, J., & Sun, T. (2019). Stable Forearc Stressed by a
958 Weak Megathrust: Mechanical and Geodynamic Implications of Stress Changes Caused by
959 the M = 9 Tohoku-Oki Earthquake. *Journal of Geophysical Research: Solid Earth*, *124*(6),
960 6179–6194. https://doi.org/10.1029/2018JB017043

961 Wang, K., & Hu, Y. (2006). Accretionary prisms in subduction earthquake cycles: The theory of
962 dynamic Coulomb wedge. *Journal of Geophysical Research: Solid Earth*, *111*(6), 6410.
963 https://doi.org/10.1029/2005JB004094

964 Wang, K., & Tréhu, A. M. (2016). Invited review paper: Some outstanding issues in the study of
965 great megathrust earthquakes—The Cascadia example. In *Journal of Geodynamics* (Vol.
966 98, pp. 1–18). Elsevier Ltd. https://doi.org/10.1016/j.jog.2016.03.010

967 Wells, R. E., Blakely, R. J., Sugiyama, Y., Scholl, D. W., & Dinterman, P. A. (2003). Basin-
968 centered asperities in great subduction zone earthquakes: A link between slip, subsidence,
969 and subduction erosion? *Journal of Geophysical Research: Solid Earth*, *108*(B10), 2507.
970 https://doi.org/10.1029/2002jb002072

971 Williamson, A. L., & Newman, A. V. (2018). Limitations of the Resolvability of Finite-Fault
972 Models Using Static Land-Based Geodesy and Open-Ocean Tsunami Waveforms. *Journal*
973 *of Geophysical Research: Solid Earth*, *123*(10), 9033–9048.
974 https://doi.org/10.1029/2018JB016091

975